Response of Subantarctic microbes to new versus regenerated Fe in a cold-core eddy

Marion Fourquez[1], Robert Strzepek[2], Michael J Ellwood[3], Christel Hassler[4], Damien Cabanes[5], Sam Eggins[6], Imojen Pearce[7], Stacy Deppeler[8], Thomas W. Trull[9], Philip W Boyd[10], and Matthieu Bressac[11]

[1]Aix Marseille Univ., Universite de Toulon
[2]University of Tasmania
[3]Australian National University
[4]University of Geneva
[5]Univ. de Geneva
[6]Research School of Earth Sciences
[7]Australian Antarctic Division, AAD, Kingston, TAS, Australia
[8]National Institute of Water and Atmospheric Research
[9]Commonwealth Scientific and Industrial Research Organisation (CSIRO)
[10]Institute for Marine and Antarctic Studies
[11]Sorbonne Université

November 22, 2022

Abstract

In the Subantarctic sector of the Southern Ocean, vertical entrainment of dissolved iron (DFe) triggers the seasonal productivity cycle. However, diminishing physical supply of new Fe during the spring to summer transition rapidly drives epipelagic microbial communities to rely upon recycled DFe for growth. Hence, subpolar waters evolve seasonally from a high fe ratio system (i.e., [uptake of new Fe]/[uptake of new+recycled Fe]) to a low fe ratio system. Here, we tested how resident microbes within a cyclonic eddy respond to different Fe/ligand inputs which mimic entrained new DFe (Fe-NEW), diffusively-supplied regenerated DFe (Fe-REG), and a control with no addition of DFe (Fe-NO). After 6 days, 3.5 (Fe-NO, Fe-NEW) to 5-fold (Fe-REG) increases in Chl a were observed despite ˜2.5-fold range between treatments of initial DFe. Marked differences were also evident in the proportion of in vitro DFe derived from recycling to sustain phytoplankton growth (Fe-REG, 30% recycled c.f. 70% Fe-NEW, 50% Fe-NO). This trend supports the concept that DFe/ligands released from subsurface particles are more bioavailable than new DFe collected at the same depth. This additional recycling may be mediated by bacteria. Indeed, by day 6 bacterial production (BP) was comparable between Fe-NO and Fe-NEW but˜2 fold higher in Fe-REG. Interestingly, a preferential response of phytoplankton (haptophyte-dominated) relative to bacteria was also found in Fe-REG. In contrast, in Fe-NEW and Fe-NO the proportion of diatoms increased. Hence, different modes of Fe/ligand supply modify BP and Fe bioavailability to phytoplankton that may drive distinctive floristic shifts and biogeochemical signatures.

Response of Subantarctic microbes to new versus regenerated Fe in a cold-core eddy

M. Fourquez[1,2,3], R. Strzepek[1,2], M.J. Ellwood[4], C. Hassler[5], D. Cabanes[5], S. Eggins[4], I. Pearce[6], S. Deppeler [1,7], T. Trull [1,2,8], P.W. Boyd [1,2] , M. Bressac[1,9]

[1] Institute for Marine and Antarctic Studies, University of Tasmania, Hobart, TAS, Australia;
[2] Antarctic Climate and Ecosystems CRC, University of Tasmania, Hobart, TAS, Australia;
[3] Aix Marseille Univ., Université de Toulon, CNRS, IRD, MIO UMR 110, 13288, Marseille, France
[4] Research School of Earth Sciences, Australian National University, Canberra, Australia;
[5] Marine and Lake Biogeochemistry, Department F.-A. Forel, University of Geneva, Geneva, Switzerland
[6] Australian Antarctic Division, AAD, Kingston, TAS, Australia;
[7] National Institute of Water and Atmospheric Research, Wellington, New Zealand;
[8] Climate Science Centre, Oceans and Atmosphere, Commonwealth Scientific and Industrial Research Organisation, Hobart, TAS, Australia.
[9]Sorbonne Université, CNRS, Laboratoire d'Océanographie de Villefranche, LOV, Villefranche-sur-Mer, 06230, France

Keywords: Fe regeneration, particles, Southern ocean eddies, vertical supply, Subantarctic

ABSTRACT

In the Subantarctic sector of the Southern Ocean, vertical entrainment of dissolved iron (DFe) triggers the seasonal productivity cycle. However, diminishing physical supply of new Fe during the spring to summer transition rapidly drives epipelagic microbial communities to rely upon recycled DFe for growth. Hence, subpolar waters evolve seasonally from a high *f*e ratio system (i.e., [uptake of new Fe]/[uptake of new+recycled Fe]) to a low *f*e ratio system. Here, we tested how resident microbes within a cyclonic eddy respond to different Fe/ligand inputs which mimic entrained new DFe (Fe-NEW), diffusively-supplied regenerated DFe (Fe-REG), and a control with no addition of DFe (Fe-NO). After 6 days, 3.5 (Fe-NO, Fe-NEW) to 5-fold (Fe-REG) increases in Chl *a* were observed despite ~2.5-fold range between treatments of initial DFe. Marked differences were also evident in the proportion of *in vitro* DFe derived from recycling to sustain phytoplankton growth (Fe-REG, 30% recycled c.f. 70% Fe-NEW,

50% Fe-NO). This trend supports the concept that DFe/ligands released from subsurface particles are more bioavailable than new DFe collected at the same depth. This additional recycling may be mediated by bacteria. Indeed, by day 6 bacterial production (BP) was comparable between Fe-NO and Fe-NEW but~2 fold higher in Fe-REG. Interestingly, a preferential response of phytoplankton (haptophyte-dominated) relative to bacteria was also found in Fe-REG. In contrast, in Fe-NEW and Fe-NO the proportion of diatoms increased. Hence, different modes of Fe/ligand supply modify BP and Fe bioavailability to phytoplankton that may drive distinctive floristic shifts and biogeochemical signatures.

Plain language summary

The Subantarctic Southern Ocean is far away from terrestrial iron inputs. Low dissolved iron (DFe) supply strongly limits the growth of phytoplankton in subpolar surface waters. However, phytoplankton benefit from vertical Fe supply from a subsurface reservoir (termed new Fe) which triggers the beginning of the phytoplankton growth season. However, this entrained new DFe is rapidly consumed and hence relief from Fe stress is only transitory. The relative influence of mid-season diffusive vertical supply and Fe recycling in supporting phytoplankton growth during the transition from new to recycled DFe remains unknown. This study uses a two-step experiment to simulate the seasonal DFe supply pathways for a resident community late in the growth season when cells should be acclimated to low DFe levels. We show that regenerated DFe from subsurface particles enhance secondary production by bacteria and stimulates specific phytoplankton taxa to grow. In particular, we present evidence that small species and non-siliceous cells were better able to take advantage of Fe regenerated from particles than large phytoplankton species. The distinctive stimulation of different microbial pathways driven by different DFe supply mechanisms provides insights into the seasonal signatures of iron biogeochemistry on the subpolar Southern Ocean.

1. INTRODUCTION

Low concentrations of dissolved iron (DFe) exert a strong influence on the primary productivity across much of the Southern Ocean (SO) (Moore et al., 2001). Nevertheless, widespread phytoplankton blooms occur every year due to the supply of dissolved Fe (DFe) over wide areas of the SO (Thomalla et al., 2011). In early spring, this Fe fertilization is dominated by a one-off pulse of new DFe from the subsurface reservoir through deep winter mixing and entrainment (Nicholson et al., 2019; Tagliabue et al., 2014). This new DFe is rapidly consumed by the upper ocean biota and, as the mixed layer (ML) depth decreases over the season, the diapycnal diffusion of regenerated DFe (from subsurface biological recycling) becomes a major mechanism to extend the duration of summertime production (Boyd et al., 2005, 2017; Tagliabue et al., 2014).

Several studies have investigated how the phytoplankton community responds to transient ML deepening (i.e. Arteaga et al., 2020; Rembauville et al., 2017) but confounding effects have hindered our understanding of biological responses to different Fe sources. For example, during late summer - when Fe limitation is at its strongest (Boyd, 2002; Mtshali et al., 2019; Ryan-Keogh et al., 2018) - the response of phytoplankton to transient ML deepening is partly controlled by the degree of Fe limitation relative to light availability (Boyd & Abraham, 2001; Fauchereau et al., 2011). Further, changes in vertical mixing can alter predator-prey interactions (Behrenfeld, 2010) and the effect of ML deepening then becomes more complex than an early season pulse of physically supplied new DFe. Organisms have therefore adapted strategies in response to seasonal changes in Fe availability. At the cellular level, upregulation of Fe transport systems (i.e. Hudson & Morel, 1990; Strzepek et al., 2011; Toulza et al., 2012) and substitution with isofunctional Fe-free proteins (Nunn et al., 2013; Saito et al., 2011; Strzepek & Harrison, 2004) increase Fe uptake rates and decrease the dependence on extracellular Fe, respectively. At the community level, intense grazing- and viral-mediated Fe recycling can account for most of the microbial Fe demand (Boyd et al., 2012; Poorvin et al., 2004; Sarthou et al., 2008; Strzepek et al., 2005).

Heterotrophic prokaryotes (here after ‘bacteria’) play a key role in DFe recycling. Particulate Fe loss during cell lysis can be solubilized in the upper water column by bacteria, which ultimately replenishes the DFe pool (Blain & Tagliabue, 2016 and references herein). Regeneration of DFe by bacteria (termed remineralization) also occurs at depth often on

sinking or suspended biogenic particles, which resupplies surface waters through vertical mixing (Boyd et al., 2017; Bressac et al., 2019; Tagliabue et al., 2014). This source of DFe relies heavily upon the efficiency of Fe recycling within the microbial loop (as termed the 'ferrous wheel', Kirchman, 1996) that can drive 50 to >90% of Fe-fueled productivity (Strzepek et al., 2005).

Within the ferrous wheel, bacteria are also pivotal in setting Fe bioavailability for the entire microbial community. Indeed, most remineralization of organic carbon in the ocean is driven by these microorganisms, a process that returns particulate Fe into dissolved forms (Boyd et al., 2010; Bressac et al., 2019) together with Fe-ligands (Christel S. Hassler et al., 2017; Hunter & Boyd, 2007). Bacteria also represent a large fraction of the biogenic Fe pool and contribute significantly to DFe utilization in the ML (Boyd et al., 2010; Fourquez et al., 2015; Strzepek et al., 2005). Rates of DFe regenerated by bacteria (Boyd et al., 2010, 2012) can effectively meet the high Fe requirements of phytoplankton (Twining & Baines, 2013). However, specific-taxon metabolic strategies amongst phytoplankton are influenced by differences in the mode of DFe supply (Boyd et al., 2017), meaning that bacterially-regenerated sources of DFe may not be bioavailable to all organisms. This raises the following questions: can acclimated surface microbial communities access regenerated Fe? And if some taxa target the supply of new Fe (Boyd et al., 2017), do others focus on recycled forms? These aspects are of particular importance in oceanic features where external Fe sources are not effective, such as persistent strong eddies in the Subantarctic Zone (SAZ; Frenger et al., 2015).

In this study, we aimed to address these questions by testing the response of in-eddy resident microbial communities to different Fe supply (and differing ligands) scenarios. Our experimental set-up was based on the seasonal variability of the *f*e ratio (i.e., the proportion of Fe uptake from new and regenerated sources, (Boyd et al., 2005). From early spring to late summer, the *f*e ratio is projected to decline along with the growing dependency of the biota to access DFe from regenerated sources (Tagliabue et al., 2014). To mimic the supply of subsurface DFe along with the alteration of predator-prey interactions, we simulated changes in top-down control of phytoplankton stocks through dilution. This approach could lead to a decoupling of the predator-prey link in the ferrous wheel. However, it was a necessary step toward investigating the physiological changes, community shifts, and competitive interactions among the different microbial groups (phytoplankton and bacteria) to different DFe sources. Hence, we followed the biological responses of the surface community to the following

perturbations: supply of subsurface upwelled new DFe (high *f*e ratio), diffusive supply from subsurface waters with regenerated DFe (intermediate *f*e ratio), and ambient surface DFe with high recycling (low *f*e ratio).

2. MATERIAL AND METHODS

2.1. Environmental context

The study was carried out in April 2016 aboard the RV *Investigator* in the Subantarctic Zone (EDDY cruise, part of the V02-IN2016 voyage from March 11 to April 17, 2016), at the center of a cyclonic cold-core eddy (50.4°S, 147.1°E; 190 km in diameter; Supp. Fig. 1). Eddies are highly variable physical-chemical features in space and time, and can become structurally closed. In late summer 2016, one of these isolated eddies detached from the Subantarctic Front (Patel et al., 2019) and was characterized by an extremely low DFe inventory (Ellwood et al., 2020) and low primary productivity (Moreau et al., 2017). This eddy was sampled in the middle of its lifetime during late summer/earlier fall when biological production is expected to be particularly sensitive to vertical entrainment of new DFe (Ryan-Keogh et al., 2018) and when microbial residents are acclimated to very low Fe concentrations (Tagliabue et al., 2014). Investigations on DFe isotopes inventory confirmed that enhanced bacterially-mediated Fe recycling occurred below 100m depth, and suggested that cells in the euphotic zone also upregulated uptake of Fe and recycling processes to sustain themselves (Ellwood et al., 2020).

The study was conducted in two steps, preparation of DFe treatments, followed by manipulation of samples to be incubated. The conceptual basis behind the design of each treatment comes from a proposed seasonal transition from high to low *f*e ratios outlined in Tagliabue et al. (2014) (see Suppl. Fig. 1). We used this approach to prepare three DFe treatments that represent the hypothetical transition of modes of DFe supply from mainly new DFe early in the season (entrainment), regenerated DFe from the recycling of subsurface materials in summer (diapycnal diffusion), and no supply of DFe (dominance of DFe recycling in surface). In addition to collecting seawater and subsurface particles (see section 2.2) at the center of the eddy (50.4°S, 147.1°E), we collected discrete seawater samples at the edge (49.7°S, 146.4°E) for comparison.

2.2.Preparation of three different DFe sources

All manipulations were carried out under strict trace metal-clean conditions in a clean container and in a laminar flow hood. Detailed cleaning procedures to prepare all the labware in trace metal-clean conditions can be found in the Geotraces Cookbook (Cutter et al., 2017).

2.2.1. Source of new DFe

To mimic supply of new DFe (entrainment), deep water samples were collected at 150m depth at the center of the eddy from trace metal clean Niskin bottles deployed on a trace metal rosette. Seawater was directly filtered from the Niskin bottles (transferred into a clean container) through an acid-cleaned 0.2-µm capsule filter (Suppl. Fig. 2).

2.2.2. Source of regenerated DFe

To mimic supply of regenerated DFe from subsurface materials (diffusion diapycnal) we collected particles at 150m depth at the center of the eddy by *in-situ* filtration (McLane Research Laboratories *in situ* pumps). A total of 345L of seawater passed through acid-leached 1.0-µm polycarbonate (PC) filters (142 mm diameter). The subsurface particles were gently resuspended in a 10L High Density Polyethylene (HDPE) acid-washed bottle containing 7L of <0.2-µm seawater (acid-cleaned 0.2-µm capsule filter Supor Acropak 200, Pall) collected at the same depth, resulting in a concentration factor of particles close to 50. For 6 days, the particles with their attached bacteria were incubated in the dark (to avoid photochemical breakdown of ligands), under gentle agitation, and at the *in situ* temperature of 7°C. We assume that (as we concentrated the particulate fraction) mainly attached bacteria were involved in the degradation of the particulates, thereby releasing DFe and ligands in the dissolved phase. The efficiency of bacterial remineralization was assessed over time by measuring total and free-living bacterial production along with changes in nutrient (NH_4, NO_2, NO_3, PO_4, and Si) concentration, including DFe.

2.2.3. Source of surface DFe

For ambient DFe source, surface seawater was collected at 5m depth at the center of the eddy using towed *in situ* sampler and directly filtered through an acid-cleaned 0.2-µm capsule filter (Supor Acropak 200, Pall).

2.2 Incubation of surface microbial community

The surface microbial community was collected from 5m depth at the center of the eddy using a towed fish system and drawn onboard using an air-driven Teflon diaphragm pump. Incubation experiments were set in acid-washed 1L round polycarbonate bottles and consisted of mixing 375 mL of surface seawater with (i) 375 mL of source of new Fe (Fe-NEW treatment), (ii) 375 mL of source of regenerated Fe (Fe-REG treatment), and (iii) 375 mL of source of surface seawater (Fe-NO treatment); leading to a systematic dilution of the surface community by 50% (Suppl. Fig. 2). Twelve independent replicates per treatment were covered with shade cloth (73 ± 5% of surface irradiance), placed in an on-deck incubator with continuous seawater supply (9.9 ± 1.1°C), and harvested after 0, 2, 4 and 6 days.

In parallel, we performed additional dark incubations of natural surface communities amended either with 1 nM $FeCl_3$ ("NO-dark +Fe") or organic carbon 10 µMC (trace metal-clean glucose, "NO-dark +C"), or a combination of both ("NO-dark +Fe+C"), and followed daily bacterial abundance and heterotrophic production for up to 6 days (Suppl. Fig. 2). Note that in the +Fe+C treatment 16.6 µmolFe $molC^{-1}$ of nutrients were added to match the bacterial Fe quota observed for Fe-replete bacterial cultures (Fourquez et al., 2014). These incubations were dedicated to determining if single and/or combined additions of Fe and C stimulate bulk and cell-specific bacterial production, and assessing if heterotrophic prokaryotes from the surface ocean were primarily Fe or C-limited. Additional incubations with Fe-NO and Fe-REG waters (NO-dark and REG-dark, respectively) were conducted under the same conditions but with no amendment to compare with products produced during the remineralization of subsurface particles (step 1). Suppl. Figure 2 summarizes the experimental set-up.

2.3. Biological metrics

The biological response of the microbial community (phytoplankton and bacteria) to the three different DFe sources were monitored from these incubation bottles, and analyzed for several parameters as described in sections below. Three biological replicates were used at each time point to get independent data points.

2.3.1. Cell abundances

Enumeration of pico- and nanophytoplankton, cyanobacteria and heterotrophic prokaryotes cells were determined by flow cytometry with similar methods and instrumentation as described in Fourquez et al. (2020). Briefly, 4.5 mL subsamples were fixed with glutaraldehyde (0.5% final concentration) in the dark at 4°C for 20 min, shock-frozen in liquid nitrogen, and

stored at -80°C. High (HNA) and low nucleic acid content (LNA) prokaryotes were discriminated depending on their respective signature in the cytogram of green fluorescence versus side scatter. Autotrophic cell populations were separated into regions based on their autofluorescence in red (FL3) versus orange (FL2) bivariate scatter plots. Cyanobacteria were determined from their high FL2 and low FL3 fluorescence. Pico- and nanophytoplankton communities were determined from their relative cell size using side scatter versus FL3 bivariate scatter plots.

2.3.2. Pigments composition

Samples (400-600 mL) for pigments were analyzed by HPLC (Wright et al., 2010). Pigments were regrouped into indices using diagnostic pigments (DP = alloxanthin (Allo)+19'-hexanoyloxyfucoxanthin (Hex)+19'-butanoyloxyfucoxanthin (But)+fucoxanthin (Fuco)+zeaxanthin (Zea)+chlorophyll b (Chlb)+peridinin (Peri)). They were used to follow the temporal evolution of the pico- (PPF=(Zea+Chlb) / DP), nano- (NPF = (Hex+But+Allo) / DP), and microphytoplankton (MPF=(Fuco+Peri) / DP) proportion factors (Hooker et al., 2005; Vidussi et al., 2001). PPF and NPF compared well with pico- (R^2=0.97, n=9) and nanophytoplankton (R^2 =0.84, n=9) cell abundances measured by flow cytometry, respectively.

2.3.3. Photochemical efficiency

The maximum quantum yield of photosystem II (Fv/Fm) was measured on a Fast Repetition Rate fluorometer (Chelsea Technologies Group Fast Ocean Sensor). Triplicate samples (20 mL) were taken from each incubation bottle and dark-adapted for 30 min. Fv/Fm (where Fv = Fm – F_0) was estimated from F_0 and Fm, which refer to the minimum and maximum fluorescence in the dark-acclimated state, respectively.

2.3.4. Secondary production

Bacterial production (BP) was estimated by the ^{3}H-Leucine incorporation method (Kirchman et al., 1985) adapted by Smith and Azam (1992) for measuring bacterial production directly in microcentrifuge tubes. Briefly, 1.5 mL samples were incubated in the dark at in situ temperature for 2–3 h with a mixture of radioactive (L-[3,4,5-3H(N)] PerkinElmer, specific activity 123.8 mCi.mol-1) and nonradioactive leucine (20 nM final concentration). Incubations were started within 10 min of collection and maintained at in situ surface temperature (13.5°C). Samples were run with two replicates and one trichloroacetic acid (TCA; Sigma)-killed control (5% [vol/vol] final concentration). At the end of the incubation time, 200 µL of 50%TCA is added to all but the control tubes to terminate leucine incorporation. Samples were centrifuged

at 16,000g for 10 min, the supernatant discarded, and the resultant precipitated cells were washed by the addition of 1.5 ml of 5% TCA and vortex mixing. Samples were centrifuged again (16,000g for 10 min) and the supernatant was removed. Subsequently, 1.5 mL of UltimaGoldTM uLLt (PerkinElmer) was added to each tubes, mixed, and allowed to sit for >24 h before the radioactivity was counted onboard in Hidex 300SL Liquid Scintillation Counter. The linearity of leucine incorporation was tested in parallel. Details for the calculation can be found in a companion paper (Fourquez et al., 2020).

2.3 Chemical analysis

Dissolved inorganic nutrients were analysed on board with a segmented flow analyser (AAIII HR Seal Analytical) according to Rees et al. (2019). Detection limits were 0.02 μM for P, 0.02 μM for N, and 0.2 μM for Si. DFe was analyzed by flow injection with online preconcentration and chemiluminescence detection (adapted from Obata et al., 1993). The detection limit was 40 pM and the accuracy of the method was controlled by analyzing the SAFe S (0.11 ± 0.04 nmol kg^{-1} (n = 3); consensus value 0.093 ± 0.008 nmol kg^{-1}), and SAFe D1 (0.66 ± 0.06 nmol kg^{-1} (n = 4); consensus value 0.67 ± 0.04 nmol kg^{-1}) standards. Iron organic speciation was measured by Competitive Ligand Exchange-Adsorptive Cathodic Stripping Voltammetry as per Abualhaija & van den Berg (2014).

3 Results and discussion

Eddie's can develop as a closed structure with no other possible inputs of DFe to the upper ocean than of new (from deep waters) or regenerated DFe (from remineralization). The contribution of new Fe to total Fe supply — the *f*e ratio (new Fe/(new + regenerated Fe) — thus can range between 6% and 50% from low- to high-DFe waters (Tagliabue et al., 2014 and refs herein). In this context, our study aimed to provide a mechanistic understanding of the biological response to ML deepening when cells are adapted to strong Fe limitation and hypothetical low *f*e ratio. To define the biological context of our experiments and to determine whether biological parameters in our experiments were similar to those sampled in the field, we start by discussing the initial conditions of our study.

3.1 Initial conditions

3.1.1 Surface

In-eddy, surface DFe levels were exceedingly low (<50 pM), and Chl *a* and primary productivity were about 1.5 and 3 times lower, respectively than surrounding Subantarctic waters (Ellwood et al., 2020; Moreau et al., 2017). We sampled the microbial community at the center of the eddy, and the photosynthetic competence of the cells was relatively high at the initial time of sampling (F_v/F_m = 0.47 ± 0.07; Fig. 1b). It is a surprising result when considering that under DFe limitation and replenished macronutrients (Suppl. Table 1), the Fv/Fm ratio decreases proportionally with the degree of Fe stress (Falkowski & Kolber, 1995; Greene et al., 1994). Nevertheless, relatively high Fv/Fm does not necessarily reflect Fe-replete conditions for cells as it can also be indicative of a 'signature' for taxonomic composition of the phytoplankton community (Suggett et al., 2009). Within the eddy, small photosynthetic cells (< 2µm) – including cyanobacteria – dominated Fe uptake in the total community (Suppl. Table 2, Ellwood et al. 2020). But for cyanobacteria F_0 does not arise from photosystem II alone, and the baseline fluorescence from phycobilisomes and photosystem I can significantly contribute to the F_0 signal (Campbell et al., 1998; Murphy et al., 2017; Simis et al., 2012). Therefore, in this context the values of fluorescence-based parameters that use F_0 in their calculation, such as Fv/Fm ratio, must be interpreted with knowledge of the composition and evolution of the community.

In-eddy, cumulative Fe uptake of phytoplankton cells was approximately four orders of magnitude higher than the diffusion supply rate of new Fe across the euphotic zone (Ellwood et al., 2020), thus cells were probably highly reliant upon recycled Fe by different members of the microbial community. In the Southern Ocean, the pool of biogenic Fe in surface waters can be recycled by the action of grazers (Strzepek et al., 2005; Sarthou et al., 2008), viruses (Bonnain et al., 2016; Poorvin et al., 2011) and bacteria (Fourquez et al., 2020; Strzepek et al., 2005). A closer look at the distribution of these classes of organisms is therefore relevant for this study. Within the mixed layer (0-100m) zooplankton abundance and biomass were substantially higher within the eddy relative to the edge (Suppl. Fig. 3). For bacteria, cell abundance was on average (0-300m) 3 times higher at the edge ($1.32\pm0.26 \times 10^6$ cells mL^{-1}, n=7) than at the center of the eddy ($0.43\pm0.22 \times 10^6$ cells mL^{-1}, n=5); and in relative to the total assemblage, the number of HNA bacteria were also found to be higher at the edge (56±11% HNA) while LNA bacteria were more prominent in the center of the Eddy (95±2% LNA). Surprisingly, BP was the highest at the center of the eddy (Suppl. Fig 4), and even more than 5 times greater than rates measured at the edge when normalized by cell abundance (Suppl. Figure 4b). This result was unexpected as it goes against the widespread theory of LNA being

inactive cells, whereas HNA are usually regarded as the active part of the bacterial group (Lebaron et al., 2001). However, high growth-specific rates for LNA in nutrient-limited waters contradict this view in the past (Zubkov et al., 2001). This marked discrepancy between the proportion of HNA and BP rates in our study demonstrate that LNA bacteria are an active part of microbial communities. One possible explanation is the profound impact of grazing on the abundance of HNA in favour of LNA (Hu et al., 2020). Importantly, these results bear the stamp of intense bacterial and grazing activities, which may have led to the recycling of Fe (and the concurrent release of Fe-binding ligands) in the upper layer.

3.1.2 Subsurface

In this study, we used freshly regenerated DFe from subsurface particles to mimic resupply via diapycnal diffusion (Fe-REG treatment, see Suppl. Fig. 1). Using particulate Fe (PFe) concentration at 150m depth (0.025nM, data not shown) in conjunction with the particle concentration factor, we estimated that 16% of the PFe was transferred to the dissolved phase after 6 days. In the natural environment, the partitioning between particulate and dissolved Fe phases can result from biotic recycling and abiotic dissolution processes. Here, there are several lines of evidence to suggest that biotic actions were at play. An increase in bacterial production (BP) for particle attached-bacteria confirms that they were metabolically active (Suppl. Fig. 5). The increase in ammonium concentration (Suppl. Fig. 5), the most commonly regenerated product (Bronk et al., 2007), further confirms that remineralization took place rapidly after the resuspension of the particles. There was also indirect evidence of relatively rapid bacterial consumption of Fe, but the quasi-linear temporal trend in DFe concentration suggests a constant release rate (Suppl. Fig 5f).

Microbial remineralization of organic matter also supplies ligands, which can form complexes with newly regenerated DFe, keeping it in solution (Boyd & Ellwood, 2010; Bressac et al., 2019). There are previous reports of the concurrent release of weak Fe-binding ligands during particle remineralization experiments (Bundy et al., 2016; Velasquez et al., 2016; Whitby et al., 2020). In these studies, grazers may have played an important role in releasing both intracellular Fe and ligands, as well as modifying their composition thereby affecting Fe chemistry and bioavailability (Boyd et al., 2005, 2012). The release of predation during the preparation of regenerated DFe source (section 2.2.2) would have altered the grazer-mediated regeneration of Fe, likely dominant within the eddy - based on microzooplankton biomass (Supp. Fig. 2) - and more broadly in the Subantarctic (Bowie et al., 2001; Boyd et al., 2005,

2010; Evans & Brussaard, 2012; Sarthou et al., 2008). Thus, we cannot rule out that the amount of DFe regenerated may have been less, relative to that *in situ*, during the incubation of particles with no grazers. However, we can reasonably assume that viral abundance was not affected by the resuspension of particles in viral-replete (i.e., <0.2 µm filtered) seawater (e.g., Cram et al., 2016). Therefore, we consider the 16% regeneration rate derived as a lower estimate, especially because a significant amount of the Fe released during the experiment (Suppl. Fig. 5-h) was observed to be rapidly assimilated by the prokaryotes present.

3.2 Biological responses

The (subsaturating) addition of DFe and nutrients with realistic stoichiometries (Table 1 and Supp. Table 1), along with the relief in grazing pressure following dilution (Landry & Hassett, 1982), reproduced well the perturbations experienced by natural communities over vast areas during ML deepening. Biological responses are driven by a range of mechanisms, which can be broadly split between phototrophic (influenced by Fe) and heterotrophic (influenced by both Fe and C) responses.

3.2.1 Phototrophic responses to Fe sources

After 2 days, there was the first evidence of acclimation of phytoplankton with an increase in Chl *a* concentration in all three treatments (Fig. 1a), and by the end of the incubation time a 3.5 (Fe-NO, Fe-NEW) to 5-fold (Fe-REG) increase in Chl *a* was observed (Fig. 1a). The Fe-REG treatment showed the highest increase in Chl *a*, which was significantly different (Student's test, p<0,01) as compared to the two other treatments. No differences in Chl *a* were found between Fe-NO and Fe-NEW over the time of the experiment (Fig.1 a). Although the initial phytoplankton community was dominated by nanophytoplankton (i.e., <20µm, 64±1%), the increase in Chl *a* by day 6 (Fig. 1a) may be attributed to an increase in the abundance of picoplankton (mainly cyanobacteria, Fig. 2c) and microplankton (i.e., >20µm). For Fe-NO and Fe-NEW, the increase in diatoms biomass was clearly apparent from elevated fucoxanthin pigment concentrations compared to initial conditions (Fig. 2 f). In Fe-REG treatment, the response of diatoms was less pronounced (Fig. 2 f) and haptophytes were overall the major components of the phytoplankton community in this treatment (57±5% by day 6). Interestingly, macronutrients concentration (Suppl. Fig. 7) showed similar trends for the three treatments. The initial conditions for the experiment had relatively elevated macronutrient concentrations (Suppl. Table 1). Thus, the phytoplankton community was likely not macronutrient limited. There was only little nitrate consumption over time, but there was significant ammonium

drawdown observed by day 2 of the experiment in all the treatments (Suppl. Fig. 7). We further note that the drawdown in ammonium was accompanied by a significant increase in HNA cells in all the incubations (Fig. 2). Among all incubation bottles and time points, the minimal value in Si concentration was 2.4 µM (Suppl. Fig. 7d) which is well above limiting levels of <1 µM reached in mid-summer in the Subantarctic (Bowie et al., 2009; Eriksen et al., 2018). In contrast, final DFe concentrations systematically reached limiting levels of ~0.1 nM (Table 1) which is consistent with the persistent decline in Fv/Fm (Fig. 1b).

While the algal responses to each treatment seem comparable considering differences in DFe concentration at T0 (Table 1), a 10-fold range of the ΔDFe/ΔChla ratio (i.e., the drawdown in DFe over the increase in Chl *a*: 0.03, 0.2 and 0.3 for Fe-NO, Fe-NEW and Fe-REG, respectively) points to very different trends. Those deviations in ΔDFe/ΔChla could reflect the capacity for luxury Fe uptake by cells (i.e. acquire Fe in excess of that required to maintain maximum growth). In-eddy, phytoplankton Fe-to-carbon uptake ratios were unusually high (Ellwood et al. 2020), indicating that cells upregulated their Fe acquisition machinery relative to carbon (Suppl. Table 2). Therefore, phytoplankton could have consumed DFe at higher rates than required when DFe level was sufficiently high without any change in biomass. Accounting for the role of the different DFe inputs (source and amounts, see Table 1) in phytoplankton growth requires the parallel consideration of DFe recycled during the 6 days of the experiment.

The relative contribution of new versus regenerated Fe to biological Fe uptake is described by the *f*e ratio (Boyd et al., 2005). Based on similar considerations, we can explore the relative contribution of DFe recycled (within the incubation bottle over the duration of the experiment) to that of the DFe pool at time zero. This information, termed here as the "apparent *f*e ratio", is also the starting point of the discussion to explain that similar DFe concentrations were measured for the three treatments by day 6 (Table 1). Since the uptake of Fe was not directly measured in our experiment, our apparent *f*e ratio is computed by comparing *in situ* Fe uptake rates measured on the natural communities during the same study in a companion paper (Ellwood et al., 2020) versus estimates of Fe recycling rates. The apparent *f*e ratio is calculated by assuming steady-state conditions and with a constant Fe uptake rate over the experiment. The total amount of Fe taken up by phytoplankton was assessed by combining the *in situ* size-fractionated Fe uptake rates (Supp. Table 2, Ellwood et al., 2020) with the development of the pico-, nano- and micro- phytoplankton biomass obtained from a diagnostic pigment criterion (section 2.3, Figure 3). The difference between the final (measured) and theoretical (estimated)

concentration of DFe in incubation bottles represents the amount of Fe recycled. Since the DFe concentration was measured at the start and end of the incubation, here we define the "net Fe uptake" as the difference between the two values:

$$Net\ DFe_{\ uptake} = DFe_{\ initial} - DFe_{\ final}$$

Where DFe initial and DFe final are the concentration of DFe measured at the start and the end of the experiment in the incubation bottle, respectively.

The "Net DFe uptake" can also be formulated as a combination of two other terms :

$$Net\ DFe_{\ uptake} = (Total\ DFe_{\ uptake} \times t) + DFe_{\ recycled}$$

Where Total DFe uptake is the amount of DFe consumed by all size-fractions (Suppl. Table 2) during the incubation time (t), and

$$DFe_{\ recycled} = DFe_{\ final} - DFe_{\ estimated}$$

and

$$DFe_{\ estimated} = DFe_{\ initial} - (Total\ DFe_{\ uptake} \times t)$$

Because experiments were conducted in a 'batch system' with no replenishment, the calculated DFe recycled also corresponds to the uptake of DFe by phytoplankton including DFe released by the recycling process that occurs in the bottles. Then, the apparent *f*e ratio is calculated according to the formula:

$$\text{apparent } f\text{e ratio} = Recycled\ DFe_{\ uptake} / Net\ DFe_{\ uptake}$$

Although variations in Fe uptake rates or the use of intracellular stored Fe might have impacted the accumulation or release of DFe (e.g., Twining et al., 2004; Wilhelm et al., 2013), this exercise highlights a wide-ranging apparent *f*e ratio: 0.3 (Fe-REG), 0.5 (Fe-NO) and 0.7 (Fe-NEW). An apparent *f*e ratio of 0.5 indicates that an equal amount of recycled DFe will be biologically consumed relative to the initial DFe concentration. In the Fe-NO treatment, equal values in DFe concentration between the initial and final time-points also underlines a perfect balance between Fe uptake and Fe recycling rates, demonstrating that the rapid *in situ* turnover time of the biotic Fe pool (<1 day; Ellwood et al., 2020) was not (or only temporally) affected by dilution, and pointing to the high resilience of the ferrous wheel.

3.2.2 Heterotrophic responses to Fe sources

Bacteria showed pronounced increases in abundance in all three treatments (Fig. 2a and b). An increase of HNA abundance (Fig. 2b) and a constant number of bacteria with low nucleic acid content (LNA) were noted during the first 4 days of incubation. The persistent increase in the relative proportion of bacteria with high nucleic acid content (HNA, section 3.4), Chl *a*, and cell abundance may indicate that the grazer population did not recover completely from dilution after 6 days of incubation (Fig. 1a and 2). The relative proportion of HNA cells increased from 2-4% at the initial time to 11% (Fe-NO) and 43-36% (Fe-NEW and Fe-REG, respectively) at day 2 and went on increasing up to about 60% by day 4 in all treatments (Fig 2b). Overall, stimulation in bacterial production rates, potentially driven by metabolically more active HNA bacteria, may have led to the recycling of Fe (and the concurrent release of Fe-binding ligands) similarly to what was observed during the preparation of Fe regenerated source from subsurface particles. Finally, we observed a decreasing trend starting on day 4 and the percentage of HNA cells accounted for less than 10% of the cells in all treatments by the end of the experiment.

Knowledge of the environmental controls on bacteria is needed to interpret these results from the three treatments. In high nutrients low chlorophyll (HNLC) regions, both Fe and C may be present at limiting concentrations for heterotrophic bacteria (Church et al., 2000; Fourquez et al., 2020; Obernosterer et al., 2015), leading to interactions among different bacterial groups to access Fe (Fourquez et al., 2012, 2016). The primary dependence of bacterial growth by one or the other element also directly influences interactions between primary producers and bacteria (Fourquez et al., 2015, 2020). In our study, an increase in BP rates were observed in the dark treatments (NO-dark, REG-dark, NO-dark +C), and the absence of stimulation after the addition of Fe (NO-dark +Fe) indicate that bacteria were primarily C-limited (Fig. 1d). The highest BP rates were observed when both C and Fe were added (NO-dark +Fe+C; Fig. 1d), supporting previous observations of increasing bacterial Fe demand when C limitation is relieved (Fourquez et al., 2014). A tight coupling between phytoplankton and bacteria biomass also confirms that bacterial growth was mainly driven by the release of phytoplankton-derived dissolved organic C (DOC) in the incubation bottles (Fig. 4). Assuming that the release of phytoplankton-derived DOC followed a trend similar to the initial DFe concentrations, the expected enhancement bacterial Fe uptake that would result in the Fe-NEW and Fe-REG treatments could explain the wide range in ΔDFe/ΔChla ratio (section 3.3.1). However, replenished organic C-conditions for bacteria also exacerbate competition for Fe with pico-nanophytoplankton cells (Fourquez et al., 2020), and fast-growing heterotrophic bacteria (i.e.

HNA) may quickly shift to Fe limitation. If this scenario occurs, the remineralisation process would be compromised which ultimately reduce the amount of Fe recycled from bacterial activities (Fourquez et al., 2020).

3.2.3 Is biogenic Fe recycled available to all biota?

The preferential response of the phytoplankton biomass relative to bacteria in the Fe-REG treatment (Fig. 4) suggests that autotrophic cells, likely haptophytes (as revealed by algal pigment data), consumed most of the added DFe. Within the eddy, the increased importance of Fe recycling favours smaller phytoplankton cells, which is reflected in terms of cell abundances, size-fractionated Fe uptake and the Fe:C uptake ratio datasets (Suppl. Table 2). Picophytoplankton cells were about 20% more abundant in Fe-REG than in the other two treatments by the end of the experiment (day 6, Fig. 2d), and this difference was significant (Student's test, $p<0,01$). Similar observations can be made for nanophytoplankton as we measured higher cell abundances in Fe-REG treatment starting from day 2 (Fig. 2e). In contrast, a relatively modest increase in the contribution of diatoms to Chl *a* biomass was observed, starting from ~15% and reaching <30% 6 days later (Fig. 2f). Interestingly, this increase was the lowest in the Fe-REG treatment, where the initial DFe concentration exceeded the putative DFe threshold of 0.2 nM required for diatoms to alleviate Fe stress (Boyd et al., 2012). This departure from theory may reflect the inability of diatoms to outcompete pico- and nanophytoplankton for regenerated DFe. Thus, despite diatoms requiring little Fe to bloom (Boyd et al., 2012; Strzepek et al., 2011, 2019) they could not access enough regenerated Fe to exploit the available macronutrients in the Fe-REG treatment (i.e. 6.07 ± 0.07 µM $SiOH_4$, Suppl. Table 1). The inability of diatoms to utilize this source of Fe, or at least at a lower rate than non-diatoms cells (i.e. smaller cells) may be attributed to their to physico-chemical disadvantages (e.g. lower surface area: ratio and diffusion rates), but it may also be due to the bioavailability of DFe following ligand complexation in the Fe-REG treatment.

At the start of the experiment, we measured the highest concentration in ligands for the Fe-REG treatment (Table 1). These ligands were present in a large excess of total DFe in the Fe-REG treatment (0.26 nM of DFe and 2.04 nM ligands) and were defined as predominantly weak ligands (log K Fe'L<12, Table 1). It should be noted that, contrary to weak ligands, strong ligands (log K Fe'L>12) decrease Fe bioavailability and are typically used to define the lower limit of Fe bioavailability in phytoplankton-based uptake assay (Lis et al., 2015). The release of both strong and weak Fe-binding ligands by the heterotrophic community were measured

during previous subsurface ocean remineralization experiments (Bundy et al., 2016; Velasquez et al., 2016). In our study, there was no detection of type L1 strong ligands by electrochemical analysis. The same analytical technique was employed in Velasquez et al. (2016) but the authors showed that it failed to detect L1 from their samples, although siderophores (which have conditional stability constants comparable to greater than L1 ligands [Vraspir & Butler, 2009]) were detected by mass spectrometry. The ligands associated with particle breakdown also tend to have lower conditional stability constants (log KFe ′L 10–12, or < 10, Boyd et al., 2010; Hassler et al., 2017). It is probable that particle-associated siderophores were present at very low concentrations in the Fe-REG treatment. Their contribution to the ligands pool may be too small compared to other weaker organic ligands to be detected by the method. Given that it is not clear what properties of ligands dictate the bioavailability of Fe, it is difficult to draw conclusions here. However, it is well admitted that a loosely defined fraction of DFe, the inorganic Fe (Fe'), can effectively be taken up by all microorganisms to support their metabolism and growth (C. S. Hassler et al., 2012; Morel et al., 2008). We calculated Fe' in all three treatments (Table 1), and although Fe' concentration represented systematically less than 1% of total DFe and was not enough to satisfy the biological demand, we still note that at initial times there was respectively 1.7 and 3 times more Fe' in Fe-REG than in Fe-NEW and Fe-NO treatments.

3.2.4 How well do bacteria to sustain phytoplankton with remineralization?

Towards the end of summer, when *f*e ratio is supposedly low, steady-state conditions are maintained by intense recycling of Fe. The short residence time of less than one day calculated in Ellwood et al. (2020) argues that Fe is being heavily trafficked within the euphotic zone. When scaled to the in-eddy inventory, such a high resilience in the ferrous wheel and the wide-ranging efficiency of Fe recycling highlights the role of bacteria. In this study we indirectly evaluate their efficiency at recycling Fe in incubations experiment. An alternative approach to exploring Fe recycling through bacterial activities is using the carbon budget. Estimates of organic C remineralization rates (C-remin = BCD/PP*100) are deduced from BP rates, bacterial carbon demand (BCD) and net primary production (NPP) rates integrated over the euphotic zone (100m). BCD was estimated assuming a bacterial growth efficiency (BGE) of 0.10 that was measured during the same study (Fourquez et al. 2020). For full details concerning the assessment of BP and BCD we refer to Fourquez et al. (2020). Here we calculate that 11% of the NPP were remineralized by heterotrophic bacteria. Assuming that the fraction

of Fe remineralized is the same as that of C (Bowie et al., 2015; Sarthou et al., 2008), we can conclude that similar fractions of NPP and Fe-demand are remineralized, and thus using the % of NPP that is remineralized and results from Fe-uptake experiments, we can obtain an estimate of Fe regeneration rate. Hence, this Fe regenerated rate was 0.94 pmol L^{-1} d^{-1} which represents about 7% of the total Fe uptake integrated over the euphotic layer (12.8 pmol L^{-1} d^{-1}, Ellwood et al. 2020), meaning that our estimate of DFe supply from remineralization cannot meet the entire Fe demand. Nevertheless, it could either meet 40% or 43% of the Fe demand by small phytoplankton cells (2-20µm – 2.35 pmol L^{-1} d^{-1}) or large phytoplankton cells (>20µm – 2.18 pmol L^{-1} d^{-1}), respectively. The timescale of Fe recycling is inextricably linked to the turnover times of the members of the microbial community, explained by growth and mortality rates. The role of grazers is partially precluded by our experimental approach but those of viruses need to be considered. Although not measured in this study, viruses, unaffected by the dilution, can contribute as much as grazers to Fe recycling in HNLC regions (Poorvin et al., 2004; Strzepek et al., 2005, Boyd and Elwood, 2010; Boyd et al., 2012). Viral lysis may rapidly lead to the remobilization of their intracellular Fe within the ferrous wheel, in agreement with the rapid turnover time of the biogenic Fe pool.

4 CONCLUSIONS

In the Southern Ocean, decades of studies have demonstrated that in addition to physical DFe supply, Fe bioavailability for cells is under tight control by chemistry. To date, describing the bioavailability of Fe in these waters relies on the accuracy of the chemical methods used to measure DFe (as referred to as bioavailable) at vanishing low concentrations. But the concept of "bioavailability" is bound to be nebulous because light, Fe speciation and kinetics, temperature, microbial interactions and adaptations are all, and more elements, intertwined into the definition. However, it is possible to indirectly constrain Fe bioavailability by tracking the biological responses to the supply of different forms of DFe and ligands. Here, we demonstrate that DFe regenerated from particles and new DFe was not beneficial to the same phytoplankton taxon. We also show that resident cells, with low *f*e ratios at the end of the summer, can rapidly shift from surface recycling to regenerated DFe or new Fe over the timescale of day. This shift in the mode of Fe recycling is partly induced by the competitive advantage of small cells (prokaryotes and picophytoplankton) to access DFe. These interspecific interactions, exacerbated by the partial relief in grazing pressure driven by the dilution from ML deepening, prevent diatoms growing and favors the rapid remobilization of intracellular Fe within the

ferrous wheel. In addition, the plasticity of the autotrophic metabolic machinery and the potential role played by bacteria, as a major component of the biotic Fe pool, can further limit the effect of vertical Fe supply. Together, these mechanisms buffer the response of phytoplankton biomass to vertical Fe supply despite extremely low ambient DFe levels in areas where control by grazing is prominent such as the Subantarctic.

Acknowledgements – This study is part of the EDDY project supported under Australian Research Council's Special Research Initiative for Antarctic Gateway Partnership (Project ID SR140300001). M.F. was funded from the European Union's Horizon 2020 research and innovation programme under the Marie Sklodowska-Curie grant agreement N° 894264 (BULLE-project). This project was also funded by a Marie Sklodowska-Curie Postdoctoral European Fellowship awarded to M.B. (European Union Seventh Framework Programme - FP7/2007-2013) under grant agreement no. PIOF-GA-2012-626734. The authors wish to thank the CSIRO Marine National Facility (MNF) for its support in the form of sea time on RV *Investigator*, support personnel, scientific equipment and data management. We particularly thank Cassie Schwanger for nutrient analyses onboard. All data and samples acquired on the voyage are made publicly available in accordance with MNF policy. The authors also wish to thank the CSIRO Hydrochemistry team, A. Davidson, and S. Moreau for their help in sample/data analyses and Ingrid Obernosterer for her valuable comments on the manuscript.

5 References

Abualhaija, M. M., & van den Berg, C. M. G. (2014). Chemical speciation of iron in seawater using catalytic cathodic stripping voltammetry with ligand competition against salicylaldoxime. *Marine Chemistry*, *164*, 60–74. https://doi.org/10.1016/J.MARCHEM.2014.06.005

Arteaga, L. A., Boss, E., Behrenfeld, M. J., Westberry, T. K., & Sarmiento, J. L. (2020). Seasonal modulation of phytoplankton biomass in the Southern Ocean. *Nature Communications*, *11*(1). https://doi.org/10.1038/s41467-020-19157-2

Behrenfeld, M. J. (2010). Abandoning Sverdrup's Critical Depth Hypothesis on phytoplankton blooms. *Ecology*, *91*(4), 977–989. https://doi.org/10.1890/09-1207.1

Blain, S., & Tagliabue, A. (2016). *Iron Cycle in Oceans*. John Wiley & Sons, Incorporated. https://doi.org/10.1002/9781119136859

Bonnain, C., Breitbart, M., & Buck, K. N. (2016). The Ferrojan horse hypothesis: Iron-virus interactions in the ocean. *Frontiers in Marine Science*, *3*(JUN), 1–11. https://doi.org/10.3389/fmars.2016.00082

Bowie, A. R., Maldonado, M. T., Frew, R. D., Croot, P. L., Achterberg, E. P., Mantoura, R. F. C., et al. (2001). The fate of added iron during a mesoscale fertilisation experiment in the Southern Ocean. *Deep Sea Research Part II: Topical Studies in Oceanography*, *48*(11–12), 2703–2743. https://doi.org/10.1016/S0967-0645(01)00015-7

Bowie, A. R., Van Der Merwe, P., Quéroué, F., Trull, T., Fourquez, M., Planchon, F., et al. (2015). Iron budgets for three distinct biogeochemical sites around the Kerguelen archipelago (Southern Ocean) during the natural fertilisation experiment KEOPS-2. *Biogeosciences*, *12*(12), 4421–4445. https://doi.org/10.5194/bg-12-4421-2015

Boyd, P. W. (2002). Environmental factors controlling phytoplankton processes in the Southern Ocean. *Journal of Phycology*, *861*, 844–861.

Boyd, P. W., & Abraham, E. R. (2001). Iron-mediated changes in phytoplankton photosynthetic competence during SOIREE. *Deep Sea Research Part II*, *48*, 2529–2550.

Boyd, P. W., & Ellwood, M. J. (2010). The biogeochemical cycle of iron in the ocean. *Nature Geoscience*, *3*(10), 675–682. https://doi.org/10.1038/ngeo964

Boyd, P. W., Law, C. S., Hutchins, D. A., Abraham, E. R., Croot, P. L., Ellwood, M., et al. (2005). FeCycle: Attempting an iron biogeochemical budget from a mesoscale SF 6 tracer experiment in unperturbed low iron waters. *Global Biogeochemical Cycles*, *19*(4), 1–13. https://doi.org/10.1029/2005GB002494

615 Boyd, P. W., Ibisanmi, E., Sander, S. G., Hunter, K. A., & Jackson, G. A. (2010).
616 Remineralization of upper ocean particles: Implications for iron biogeochemistry.
617 *Limnology and Oceanography*, *55*(3), 1271–1288. Retrieved from
618 http://www.aslo.org/lo/toc/vol_55/issue_3/1271.html
619 Boyd, P. W., Arrigo, K. R., Strzepek, R., & Van Dijken, G. L. (2012). Mapping phytoplankton
620 iron utilization: Insights into Southern Ocean supply mechanisms. *Journal of Geophysical*
621 *Research: Oceans*, *117*(C6), n/a-n/a. https://doi.org/10.1029/2011JC007726
622 Boyd, P. W., Ellwood, M. J., Tagliabue, A., & Twining, B. S. (2017). Biotic and abiotic
623 retention, recycling and remineralization of metals in the ocean. *Nature Geoscience*,
624 *10*(3), 167–173. https://doi.org/10.1038/ngeo2876
625 Bressac, M., Guieu, C., Ellwood, M. J., Tagliabue, A., Wagener, T., Laurenceau-Cornec, E.
626 C., et al. (2019). Resupply of mesopelagic dissolved iron controlled by particulate iron
627 composition. *Nature Geoscience 2019 12:12*, *12*(12), 995–1000.
628 https://doi.org/10.1038/s41561-019-0476-6
629 Bronk, D. A., See, J. H., Bradley, P., & Killberg, L. (2007). DON as a source of bioavailable
630 nitrogen for phytoplankton. *Biogeosciences*, *4*(3), 283–296. https://doi.org/10.5194/BG-
631 4-283-2007
632 Bundy, R. M., Jiang, M., Carter, M., & Barbeau, K. A. (2016). Iron-binding ligands in the
633 Southern California current system: Mechanistic studies. *Frontiers in Marine Science*,
634 *3*(MAR), 1–17. https://doi.org/10.3389/fmars.2016.00027
635 Campbell, D., Hurry, V., Clarke, A. K., Gustafsson, P., & Öquist, G. (1998). Chlorophyll
636 fluorescence analysis of cyanobacterial photosynthesis and acclimation. *Microbiology*
637 *and Molecular Biology Reviews : MMBR*, *62*(3), 667–683.
638 https://doi.org/10.1128/MMBR.62.3.667-683.1998
639 Church, M. J., Hutchins, D. A., & Ducklow, H. W. (2000). Limitation of bacterial growth by
640 dissolved organic matter and iron in the Southern Ocean. *Applied and Environmental*
641 *Microbiology*, *66*(2), 455–466. https://doi.org/10.1128/AEM.66.2.455-466.2000
642 Cram, J. A., Parada, A. E., & Fuhrman, J. A. (2016). Dilution reveals how viral lysis and
643 grazing shape microbial communities. *Limnology and Oceanography*, *61*(3), 889–905.
644 https://doi.org/10.1002/LNO.10259
645 Cutter, G., Sciences, A., Dominion, O., Casciotti, K., Croot, P., Sciences, O., et al. (2017).
646 Sampling and Sample-handling Protocols for GEOTRACES Cruises, (August).
647 Ellwood, M. J., Strzepek, R. F., Strutton, P. G., Trull, T. W., Fourquez, M., & Boyd, P. W.
648 (2020). Distinct iron cycling in a Southern Ocean eddy. *Nature Communications*, *11*(1).

https://doi.org/10.1038/s41467-020-14464-0

Evans, C., & Brussaard, C. P. D. (2012). Viral lysis and microzooplankton grazing of phytoplankton throughout the Southern Ocean. *Limnology and Oceanography*, *57*(6), 1826–1837. https://doi.org/10.4319/LO.2012.57.6.1826

Falkowski, P. G., & Kolber, Z. (1995). Variations in Chlorophyll Fluorescence Yields in Phytoplankton in the World Oceans. *Functional Plant Biology*, *22*(2), 341–355. https://doi.org/10.1071/PP9950341

Fauchereau, N., Tagliabue, A., Bopp, L., Monteiro, P., & S Monteiro, P. M. (2011). The response of phytoplankton biomass to transient mixing events in the Southern Ocean The response of phyto-plankton biomass to transient mixing events in the The response of phytoplankton biomass to transient mixing events in the Southern Ocean. *Geophysical Research Letters*, *38*(17). https://doi.org/10.1029/2011GL048498ï

Fourquez, M., Obernosterer, I., & Blain, S. (2012). A method for the use of the radiotracer 55Fe for microautoradiography and CARD-FISH of natural bacterial communities. *FEMS Microbiology Letters*, *337*(2), 132–139. https://doi.org/10.1111/1574-6968.12022

Fourquez, M., Schaumann, A., Gueneugues, A., Jouenne, T., & Obernosterer, I. (2014). Effects of iron limitation on growth and carbon metabolism in oceanic and coastal heterotrophic bacteria. *Limnology and Oceanography*, *59*(1), 1–14. https://doi.org/10.4319/lo.2014.59.1.0000

Fourquez, M., Obernosterer, I., Davies, D. M., Trull, T. W., & Blain, S. (2015). Microbial iron uptake in the naturally fertilized waters in the vicinity of the Kerguelen Islands: phytoplankton–bacteria interactions. *Biogeosciences*. https://doi.org/10.5194/bg-12-1893-2015

Fourquez, M., Beier, S., Jongmans, E., Hunter, R., & Obernosterer, I. (2016). Uptake of Leucine, Chitin, and Iron by Prokaryotic Groups during Spring Phytoplankton Blooms Induced by Natural Iron Fertilization off Kerguelen Island (Southern Ocean). *Frontiers in Marine Science*, *3*, 256. https://doi.org/10.3389/fmars.2016.00256

Fourquez, M., Bressac, M., Deppeler, S. L., Ellwood, M., Obernosterer, I., Trull, T. W., et al. (2020). Microbial Competition in the Subpolar Southern Ocean : An Fe – C Co-limitation Experiment. *Frontiers in Marine Science*, *6*(January), 776. https://doi.org/10.3389/fmars.2019.00776

Frenger, I., Münnich, M., Gruber, N., & Knutti, R. (2015). Southern Ocean eddy phenomenology. *Journal of Geophysical Research: Oceans*, *120*(11), 7413–7449. https://doi.org/10.1002/2015JC011047

683 Greene, R. M., Kolber, Z. S., Swift, D. G., Tindale, N. W., & Falkowski, P. G. (1994).
684 Physiological limitation of phytoplankton photosynthesis in the eastern equatorial Pacific
685 determined from variability in the quantum yield of fluorescence. *Limnology and*
686 *Oceanography*, *39*(5), 1061–1074. https://doi.org/10.4319/LO.1994.39.5.1061
687 Hassler, C. S., Schoemann, V., Boye, M., Tagliabue, A., Rozmarynowycz, M., & Mckay, R.
688 M. L. (2012). Iron bioavailability in the southern ocean. *Oceanography and Marine*
689 *Biology: An Annual Review*, *50*, 1–64. https://doi.org/10.1201/B12157-3/IRON-
690 BIOAVAILABILITY-SOUTHERN-OCEAN-HASSLER-SCHOEMANN-BOYE-
691 TAGLIABUE-ROZMARYNOWYCZ-MCKAY
692 Hassler, Christel S., van den Berg, C. M. G., & Boyd, P. W. (2017). Toward a regional
693 classification to provide a more inclusive examination of the ocean biogeochemistry of
694 iron-binding ligands. *Frontiers in Marine Science*, *4*(FEB).
695 https://doi.org/10.3389/fmars.2017.00019
696 Hooker, S. B., Van Heukelem, L., Thomas, C. S., Claustre, H., Ras, J., Barlow, R., et al. (2005).
697 The Second SeaWiFS HPLC Analysis Round-Robin Experiment (SeaHARRE-2).
698 *National Aeronautics and Space Administration, Goddard Space Flight Center.*, *212785*,
699 112. Retrieved from http://www.sti.nasa.gov/STI-homepage.html
700 Hu, C., Chen, X., Yu, L., Xu, D., & Jiao, N. (2020). Elevated Contribution of Low Nucleic
701 Acid Prokaryotes and Viral Lysis to the Prokaryotic Community Along the Nutrient
702 Gradient From an Estuary to Open Ocean Transect. *Frontiers in Microbiology*,
703 *11*(December), 1–14. https://doi.org/10.3389/fmicb.2020.612053
704 Hudson, R. J. M., & Morel, F. M. M. (1990). Iron transport in marine phytoplankton: Kinetics
705 of cellular and medium coordination reactions. *Limnology and Oceanography*, *35*(5),
706 1002–1020.
707 Hunter, K. A., & Boyd, P. W. (2007). Iron-binding ligands and their role in the ocean
708 biogeochemistry of iron. *Environmental Chemistry*, *4*(4), 221.
709 https://doi.org/10.1071/EN07012
710 Kirchman, D. L. (1996). Microbial ferrous wheel. *Nature*, *383*, 303–304.
711 Kirchman, D. L., K'nees, E., & Hodson, R. (1985). Leucine incorporation and its potential as
712 a measure of protein synthesis by bacteria in natural aquatic systems. *Applied and*
713 *Environmental Microbiology*, *49*(3), 599–607. Retrieved from
714 http://www.pubmedcentral.nih.gov/articlerender.fcgi?artid=373556&tool=pmcentrez&r
715 endertype=abstract
716 Landry, M. R., & Hassett, R. P. (1982). Estimating the grazing impact of marine micro-

717 zooplankton. *Marine Biology 1982 67:3*, *67*(3), 283–288.
718 https://doi.org/10.1007/BF00397668
719 Lebaron, P., Servais, P., Agogué, H., Courties, C., & Joux, F. (2001). Does the high nucleic
720 acid content of individual bacterial cells allow us to discriminate between active cells and
721 inactive cells in aquatic systems? *Applied and Environmental Microbiology*, *67*(4), 1775–
722 1782. https://doi.org/10.1128/AEM.67.4.1775-1782.2001
723 Lis, H., Shaked, Y., Kranzler, C., Keren, N., & Morel, F. M. M. (2015). Iron bioavailability to
724 phytoplankton: an empirical approach. *ISME Journal*, *9*(4), 1003–1013.
725 https://doi.org/10.1038/ismej.2014.199
726 Moore, J., Doney, S., Glover, D., & Fung, I. (2001). Iron cycling and nutrient-limitation
727 patterns in surface waters of the World Ocean. *Deep Sea Research Part II*, *49*(1–3), 463–
728 507. Retrieved from http://linkinghub.elsevier.com/retrieve/pii/S0967064501001096
729 Moreau, S., Penna, A. Della, Llort, J., Patel, R., Langlais, C., Boyd, P. W., et al. (2017). Eddy-
730 induced carbon transport across the Antarctic Circumpolar Current. *Global*
731 *Biogeochemical Cycles*, *31*(9), 1368–1386. https://doi.org/10.1002/2017GB005669
732 Morel, F. M. M., Kustka, A. B., & Shaked, Y. (2008). The role of unchelated Fe in the iron
733 nutrition of phytoplankton. *Limnology and Oceanography*, *53*(1), 400–404.
734 Mtshali, T. N., van Horsten, N. R., Thomalla, S. J., Ryan-Keogh, T. J., Nicholson, S. A.,
735 Roychoudhury, A. N., et al. (2019). Seasonal Depletion of the Dissolved Iron Reservoirs
736 in the Sub-Antarctic Zone of the Southern Atlantic Ocean. *Geophysical Research Letters*,
737 *46*(8), 4386–4395. https://doi.org/10.1029/2018GL081355
738 Murphy, C. D., Ni, G., Li, G., Barnett, A., Xu, K., Grant-Burt, J., et al. (2017). Quantitating
739 active photosystem II reaction center content from fluorescence induction transients.
740 *Limnology and Oceanography: Methods*, *15*(1), 54–69.
741 https://doi.org/10.1002/LOM3.10142
742 Nicholson, S. A., Lévy, M., Jouanno, J., Capet, X., Swart, S., & Monteiro, P. M. S. (2019).
743 Iron Supply Pathways Between the Surface and Subsurface Waters of the Southern Ocean:
744 From Winter Entrainment to Summer Storms. *Geophysical Research Letters*, *46*(24),
745 14567–14575. https://doi.org/10.1029/2019GL084657
746 Nunn, B. L., Faux, J. F., Hippmann, A. a., Maldonado, M. T., Harvey, H. R., Goodlett, D. R.,
747 et al. (2013). Diatom Proteomics Reveals Unique Acclimation Strategies to Mitigate Fe
748 Limitation. *PLoS ONE*, *8*(10), e75653. https://doi.org/10.1371/journal.pone.0075653
749 Obernosterer, I., Fourquez, M., & Blain, S. (2015). Fe and C co-limitation of heterotrophic
750 bacteria in the naturally fertilized region off the Kerguelen Islands. *Biogeosciences*,

751 *12*(11), 1983–1992. https://doi.org/10.5194/bg-12-1983-2015
752 Patel, R. S., Phillips, H. E., Strutton, P. G., Lenton, A., & Llort, J. (2019). Meridional Heat and
753 Salt Transport Across the Subantarctic Front by Cold-Core Eddies. *Journal of*
754 *Geophysical Research: Oceans*, *124*(2), 981–1004.
755 https://doi.org/10.1029/2018JC014655
756 Poorvin, L., Rinta-Kanto, J. M., Hutchins, D. A., & Wilhelm, S. W. (2004). Viral release of
757 iron and its bioavailability to marine plankton. *Limnology and Oceanography*, *49*(5),
758 1734–1741. https://doi.org/10.4319/lo.2004.49.5.1734
759 Poorvin, L., Sander, S. G., Velasquez, I., Ibisanmi, E., LeCleir, G. R., & Wilhelm, S. W. (2011).
760 A comparison of Fe bioavailability and binding of a catecholate siderophore with virus-
761 mediated lysates from the marine bacterium Vibrio alginolyticus PWH3a. *Journal of*
762 *Experimental Marine Biology and Ecology*, *399*(1), 43–47.
763 https://doi.org/10.1016/J.JEMBE.2011.01.016
764 Rembauville, M., Briggs, N., Ardyna, M., Uitz, J., Catala, P., Penkerc'h, C., et al. (2017).
765 Plankton Assemblage Estimated with BGC-Argo Floats in the Southern Ocean:
766 Implications for Seasonal Successions and Particle Export. *Journal of Geophysical*
767 *Research: Oceans*, *122*(10), 8278–8292. https://doi.org/10.1002/2017JC013067
768 Ryan-Keogh, T. J., Thomalla, S. J., Little, H., & Melanson, J. R. (2018). Seasonal regulation
769 of the coupling between photosynthetic electron transport and carbon fixation in the
770 Southern Ocean. *Limnology and Oceanography*, *63*(5), 1856–1876.
771 https://doi.org/10.1002/lno.10812
772 Saito, M. A., Bertrand, E. M., Dutkiewicz, S., Bulygin, V. V, Moran, D. M., Monteiro, F. M.,
773 et al. (2011). Iron conservation by reduction of metalloenzyme inventories in the marine
774 diazotroph *Crocosphaera watsonii*. *Proceedings of the National Academy of Sciences of*
775 *the United States of America*, *108*(6), 2184–2189.
776 https://doi.org/10.1073/pnas.1006943108
777 Sarthou, G., Vincent, D., Christaki, U., Obernosterer, I., Timmermans, K. R., & Brussaard, C.
778 P. D. (2008). The fate of biogenic iron during a phytoplankton bloom induced by natural
779 fertilisation: Impact of copepod grazing. *Deep Sea Research Part II*, *55*(5–7), 734–751.
780 https://doi.org/10.1016/j.dsr2.2007.12.033
781 Simis, S. G. H., Huot, Y., Babin, M., Seppälä, J., & Metsamaa, L. (2012). Optimization of
782 variable fluorescence measurements of phytoplankton communities with cyanobacteria.
783 *Photosynthesis Research*, *112*(1), 13–30. https://doi.org/10.1007/S11120-012-9729-
784 6/FIGURES/12

785 Smith, D. C., & Azam, F. (1992). A simple , economical method for measuring bacterial protein
786 synthesis rates in seawater using 3H-leucine. *Marine Microbial Food Webs*, *6*(2), 107–
787 114.
788 Strzepek, R. F., & Harrison, P. J. (2004). Photosynthetic architecture differs in coastal and
789 oceanic diatoms. *Nature*, *403*, 689–692. https://doi.org/10.1038/nature02954
790 Strzepek, R. F., Maldonado, M. T., Higgins, J. L., Hall, J., Safi, K., Wilhelm, S. W., & Boyd,
791 P. W. (2005). Spinning the "Ferrous Wheel": The importance of the microbial community
792 in an iron budget during the FeCycle experiment. *Global Biogeochemical Cycles*, *19*(4),
793 1–14. https://doi.org/10.1029/2005GB002490
794 Strzepek, R. F., Maldonado, M. T., Hunter, K. A., Frew, R. D., & Boyd, P. W. (2011). Adaptive
795 strategies by Southern Ocean phytoplankton to lessen iron limitation: Uptake of
796 organically complexed iron and reduced cellular iron requirements. *Limnology and*
797 *Oceanography*, *56*(6), 1983–2002. https://doi.org/10.4319/lo.2011.56.6.1983
798 Strzepek, R. F., Boyd, P. W., & Sunda, W. G. (2019). Photosynthetic adaptation to low iron,
799 light, and temperature in Southern Ocean phytoplankton. *Proceedings of the National*
800 *Academy of Sciences of the United States of America*, *116*(10), 4388–4393.
801 https://doi.org/10.1073/pnas.1810886116
802 Suggett, D. J., Moore, C. M., Hickman, A. E., & Geider, R. J. (2009). Interpretation of fast
803 repetition rate (FRR) fluorescence: Signatures of phytoplankton community structure
804 versus physiological state. *Marine Ecology Progress Series*, *376*(May 2014), 1–19.
805 https://doi.org/10.3354/meps07830
806 Tagliabue, A., Sallée, J. B., Bowie, A. R., Lévy, M., Swart, S., & Boyd, P. W. (2014). Surface-
807 water iron supplies in the Southern Ocean sustained by deep winter mixing. *Nature*
808 *Geoscience*, *7*(4), 314–320. https://doi.org/10.1038/ngeo2101
809 Thomalla, S. J., Fauchereau, N., Swart, S., & Monteiro, P. M. S. (2011). Regional scale
810 characteristics of the seasonal cycle of chlorophyll in the Southern Ocean.
811 *Biogeosciences*, *8*(10), 2849–2866. https://doi.org/10.5194/BG-8-2849-2011
812 Toulza, E., Tagliabue, A., Blain, S., & Piganeau, G. (2012). Analysis of the global ocean
813 sampling (GOS) project for trends in iron uptake by surface ocean microbes. *PloS One*,
814 *7*(2), e30931. https://doi.org/10.1371/journal.pone.0030931
815 Twining, B. S., & Baines, S. B. (2013). The trace metal composition of marine phytoplankton.
816 *Annual Review of Marine Science*, *5*, 191–215. https://doi.org/10.1146/annurev-marine-
817 121211-172322
818 Velasquez, I. B., Ibisanmi, E., Maas, E. W., Boyd, P. W., Nodder, S., & Sander, S. G. (2016).

819 Ferrioxamine siderophores detected amongst iron binding ligands produced during the
820 remineralization of marine particles. *Frontiers in Marine Science*, *3*(SEP), 1–14.
821 https://doi.org/10.3389/fmars.2016.00172
822 Vidussi, F., Claustre, H., Manca, B. B., Luchetta, A., & Marty, J. C. (2001). Phytoplankton
823 pigment distribution in relation to upper thermocline circulation in the eastern
824 Mediterranean Sea during winter. *Journal of Geophysical Research: Oceans*, *106*(C9),
825 19939–19956. https://doi.org/10.1029/1999JC000308
826 Vraspir, J. M., & Butler, A. (2009). Chemistry of Marine Ligands and Siderophores. *Annual*
827 *Review of Marine Science*, *1*(1), 43–63. Retrieved from
828 http://www.annualreviews.org/doi/abs/10.1146/annurev.marine.010908.163712
829 Whitby, H., Bressac, M., Sarthou, G., Ellwood, M. J., Guieu, C., & Boyd, P. W. (2020).
830 Contribution of Electroactive Humic Substances to the Iron-Binding Ligands Released
831 During Microbial Remineralization of Sinking Particles. *Geophysical Research Letters*,
832 *47*(7). https://doi.org/10.1029/2019GL086685
833 Wright, S. W., van den Enden, R. L., Pearce, I., Davidson, A. T., Scott, F. J., & Westwood, K.
834 J. (2010). Phytoplankton community structure and stocks in the Southern Ocean (30–
835 80°E) determined by CHEMTAX analysis of HPLC pigment signatures. *Deep Sea*
836 *Research Part II: Topical Studies in Oceanography*, *57*(9–10), 758–778.
837 https://doi.org/10.1016/J.DSR2.2009.06.015
838 Zubkov, M. V., Fuchs, B. M., Burkill, P. H., & Amann, R. (2001). Comparison of Cellular and
839 Biomass Specific Activities of Dominant Bacterioplankton Groups in Stratified Waters of
840 the Celtic Sea. *Applied and Environmental Microbiology*, *67*(3–12), 5210–5218.
841 https://doi.org/10.1128/AEM.67.11.5210-5218.2001
842

Table 1. Initial and final concentrations in dissolved iron (DFe), inorganic Fe (Fe'), total iron-binding ligand (L_T), and conditional stability constants (log $K'_{Fe'L}$). Values within parentheses correspond to the standard deviation of the mean of three measurements. ND denotes no data.

	DFe (nM)		LT (nM)		Log K'Fe'L		Fe' (pM)	
Treatment	Initial	Final	Initial	Final	Initial	Final	Initial	Final
Fe-NO	0.11 (0.01)	0.11 (0.01)	1.36 (0.13)	ND	11.0 (0.3)	ND	0.80 (0.1)	ND
Fe-NEW	0.16 (0.04)	0.09 (0.01)	1.69 (0.21)	ND	10.8 (0.3)	ND	1.49 (0.4)	ND
Fe-REG	0.26 (0.02)	0.10 (0.01)	2.04 (0.11)	ND	10.7 (0.2)	ND	2.52 (0.1)	ND

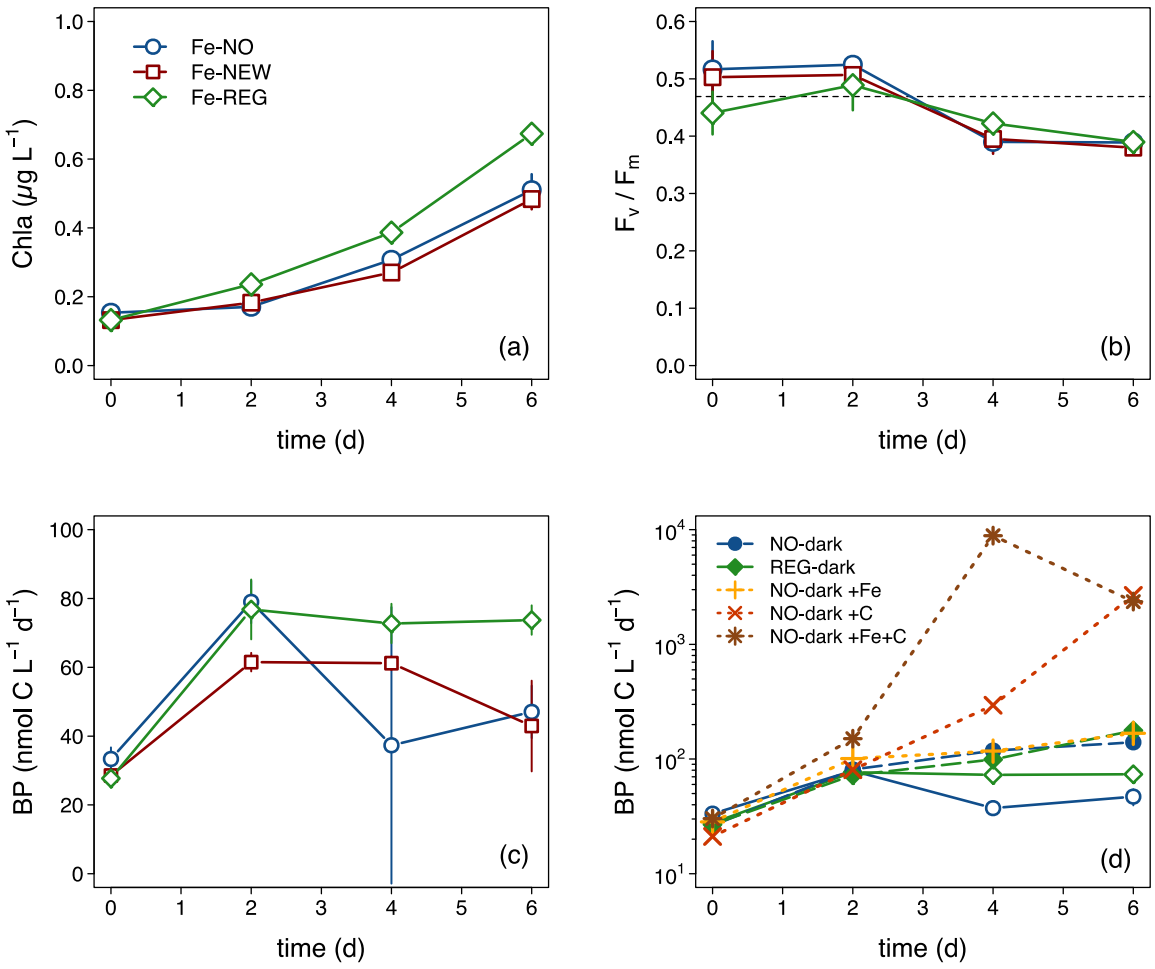

Figure 1. Time evolution of **(a)** Chla concentration, **(b)** Fv/Fm ratio, and (**c**) bacterial production (BP) for the three treatments. The horizontal dotted line in (**b**) corresponds to the *in situ* Fv/Fm ratio. (**d**) Time evolution of BP for Fe-NO and Fe-REG incubated under light and dark (NO-dark, REG-dark) conditions, and for amended (+Fe, +C, +Fe+C) NO-dark treatments. Note the logarithmic scale for the y-axis in (**d**). Error bars represent the standard deviation of three incubation bottle replicates.

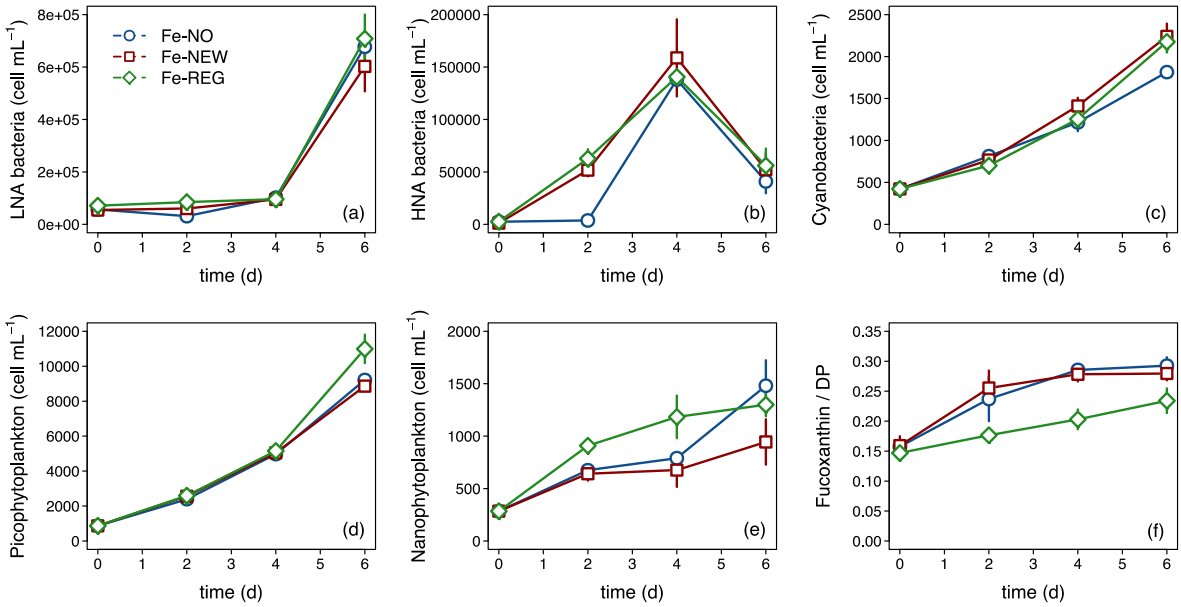

Figure 2. Time evolution of the abundance of (**a**) LNA bacteria, (**b**) HNA bacteria, (**c**) cyanobacteria, (**d**) picophytoplankton, and (**e**) nanophytoplankton measured by flow cytometry. (**f**) Time evolution of the Fucoxanthin/DP ratio, a proxy of the relative proportion of diatoms to total algal biomass derived from pigment analysis (section 2.2). Error bars represent the standard deviation of three incubation bottle replicates.

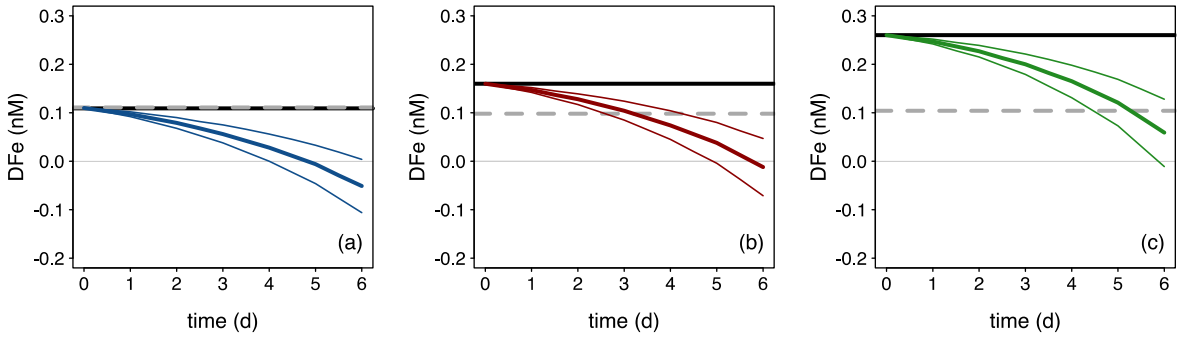

Figure 3. Theoretical evolution of DFe driven by phytoplankton uptake (colored curves) for the (**a**) Fe-NO, (**b**) Fe-NEW, and (**c**) Fe-REG treatments. Theoretical evolutions of DFe are represent in color lines: blue, red and green for the Fe-NO, Fe-NEW and Fe-REG treatments, respectively and were obtained by combining the *in situ* size-fractionated Fe uptakes rates (Supp. Table 2) with the evolution of the pico-, nano- and microphytoplankton biomass obtained from a diagnostic pigment criteria (section 2.2). The black and grey-dotted lines represent the measured initial and final DFe concentrations, respectively.

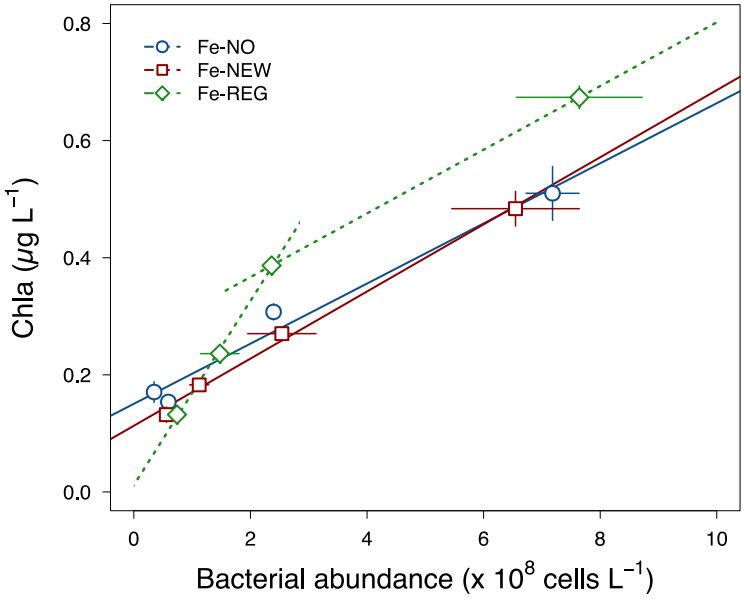

Figure 4. Relationship between Chla concentration and bacterial abundance (HNA+LNA) for the three treatments. The best-fit lines of the linear models are plotted (Fe-NO: slope = 5.1 ± 0.6 10^{-10}, R^2 = 0.98, p = 0.01; Fe-NEW: slope = 5.7 ± 0.3 10^{-10}, R^2 = 0.99, p= 0.002; Fe-REG day 0-4: slope = 15.7 ± 0.8 10^{-10}, R^2 = 0.99, p = 0.3; Fe-REG day 4-6: slope = 5.4 10^{-10}). Error bars represent the standard deviation of three incubation bottle replicates.

Suppl. Table 1. Initial biogeochemical conditions for the Fe-NO, Fe-NEW, and Fe-REG treatments.

	Fe-NO	**Fe-NEW**	**Fe-REG**
Ammonium (μM)	1.22 ± 0.16	0.72 ± 0.24	1.03 ± 0.34
Nitrate (μM)	22.36 ± 0.76	23.26 ± 0.17	23.20 ± 0.03
Nitrite (μM)	0.35 ± 0.07	0.44 ± 0.01	0.45 ± 0.01
Phosphate (μM)	1.62 ± 0.06	1.68 ± 0.01	1.69 ± 0.01
Silicate (μM)	3.16 ± 0.08	5.43 ± 0.01	6.07 ± 0.07
Dissolved iron (nM)	0.11 ± 0.01	0.16 ± 0.04	0.26 ± 0.02
Chlorophyll-a (μg L^{-1})	0.154 ± 0.016	0.132 ± 0.015	0.132 ± 0.003
F_v/F_m	0.52 ± 0.05	0.50 ± 0.05	0.44 ± 0.04

Suppl. Table 2. Iron and carbon uptake rates for the different components of the in-eddy phytoplankton community (from companion paper Ellwood et al. 2020).

	0.2-2-μm [a,b]	2-20-μm [a,b]	>20-μm [a,b]
Fe uptake (pmol L^{-1} d^{-1})	17.4 (5.6)	4.6 (3.0)	4.9 (1.2)
C uptake (μmol L^{-1} d^{-1})	0.06 (0.01)	0.05 (0.03)	0.04 (0.01)
Fe:C ratio (μmol mol^{-1})	285.4 (92.5)	99.6 (88.9)	120.6 (43.3)

[a] incubation at 80% incident irradiance; [b] extracellular Fe removed using Ti(III) EDTA-citrate

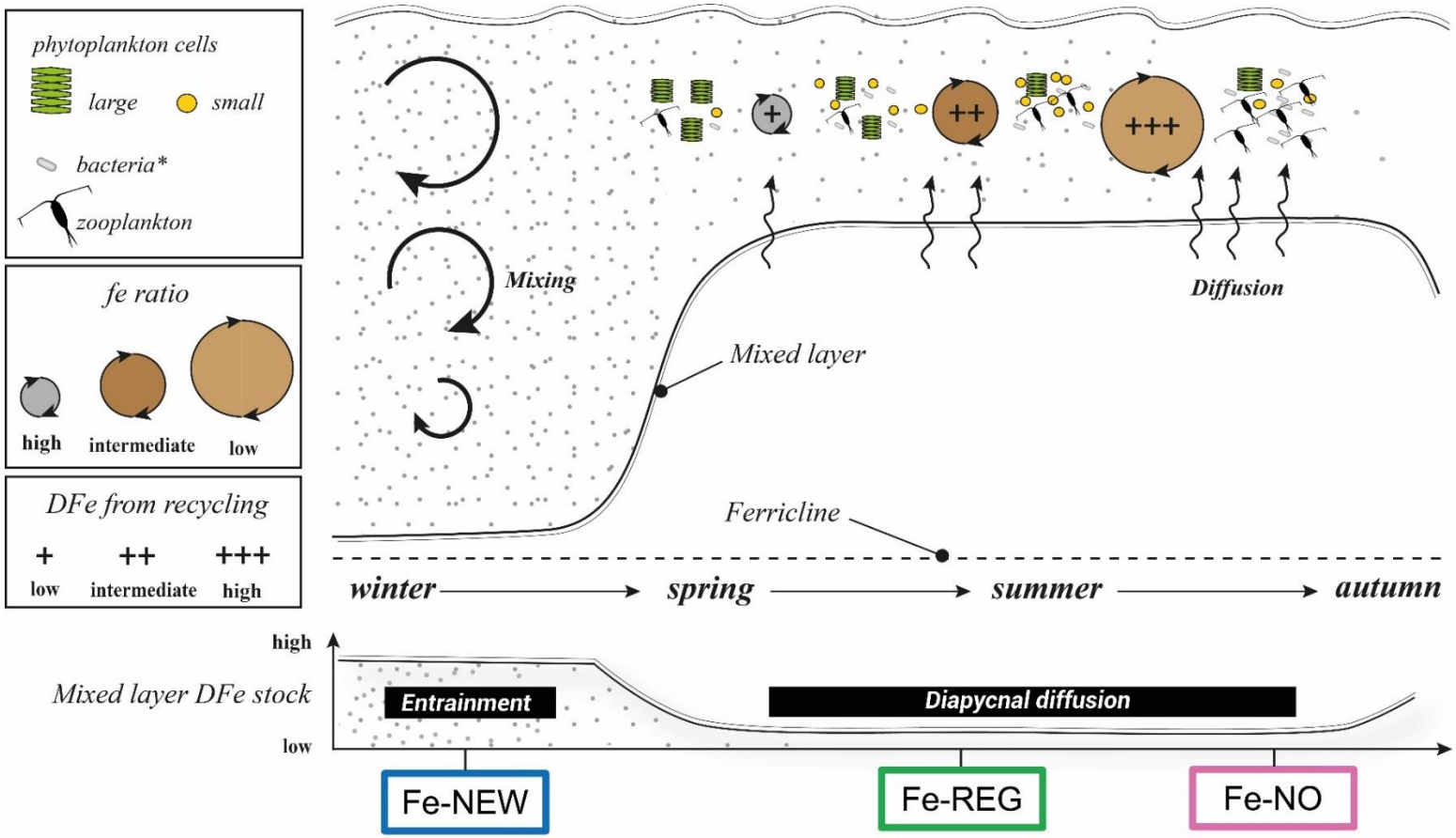

Suppl. Figure 1 A schematic representation of the seasonal variability in Southern Ocean Fe cycling adapted from Tagliabue et al. 2014. Seasonal changes in the physical supply of DFe (black arrows), mixed-layer depth and the mixed-layer DFe inventory are emphasized. The magnitude of recycling and changes in *f*e ratio are presented together (circles and cross) as well as a simplified view of the pelagic community composition. The dominant physical processes over the season is conceptualized at the bottom of the figure with the evolution of DFe inventories in the mixed layer. DFe sources (Fe-NEW, Fe-REG, and Fe-NO) used in this study aim to represent the seasonal transition of modes of DFe supply from mainly new DFe early in the season (entrainment) to regenerated DFe from recycle of sinking materials later during the summer (diapycnal diffusion) and no DFe supply.

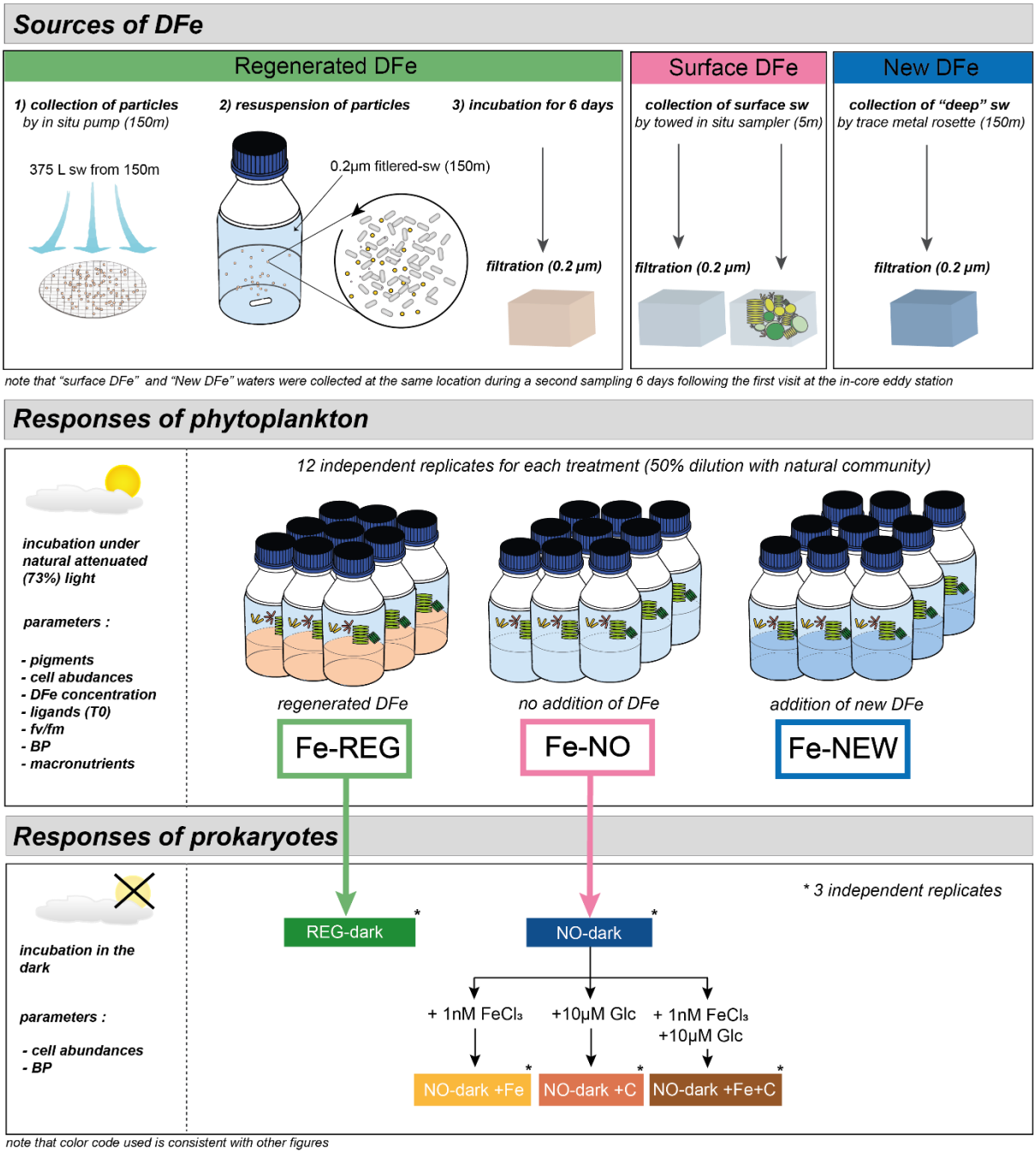

Suppl. Figure 2. A schematic representation of the experimental set-up.

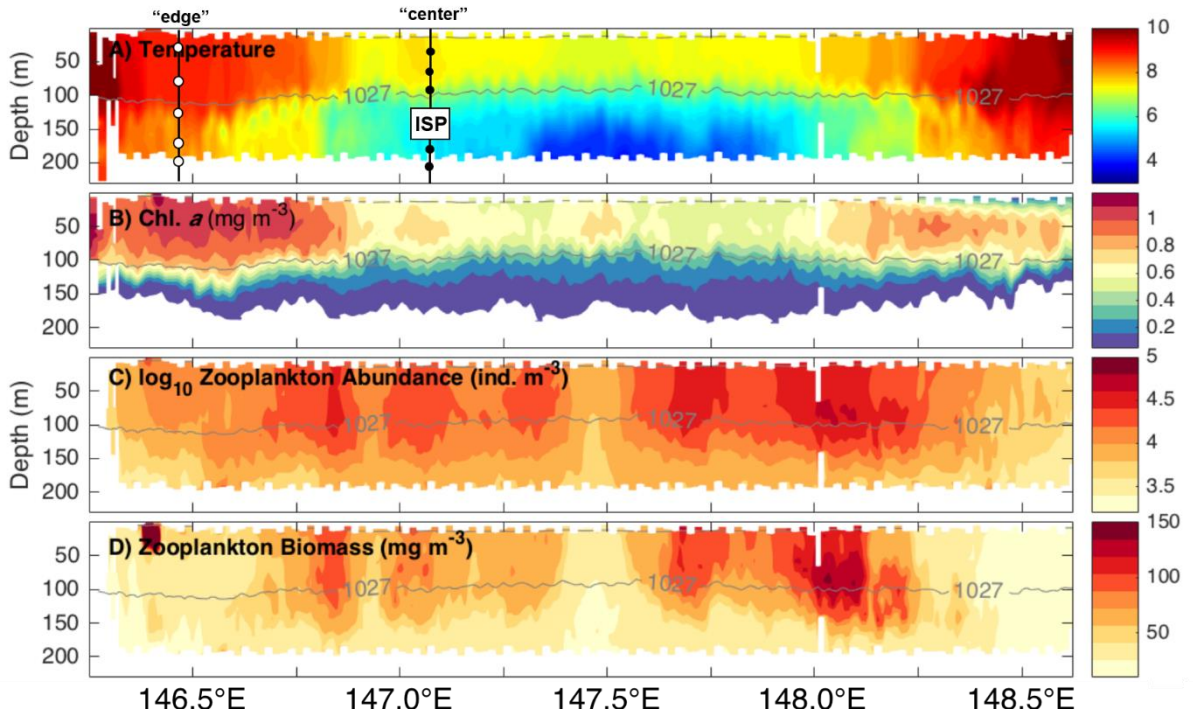

Suppl. Figure 3 (**a**) Temperature, (**b**) Chl a concentration, and zooplankton (**c**) abundance and (**d**) biomass (obtained from a Laser Optical Plankton Recorder) within the cold-core eddy and at the eddy's periphery. Location of the sampling for bacterial production profiles at the periphery ("edge", white dots) and at the within the eddy ("center", black dots) are shown in (a) panel. Sampling for surface (5m) microbial community was done at same location within the eddy ("center") as the collection of subsurface particles by In Situ Pump (ISP) deployed at 150m depth.

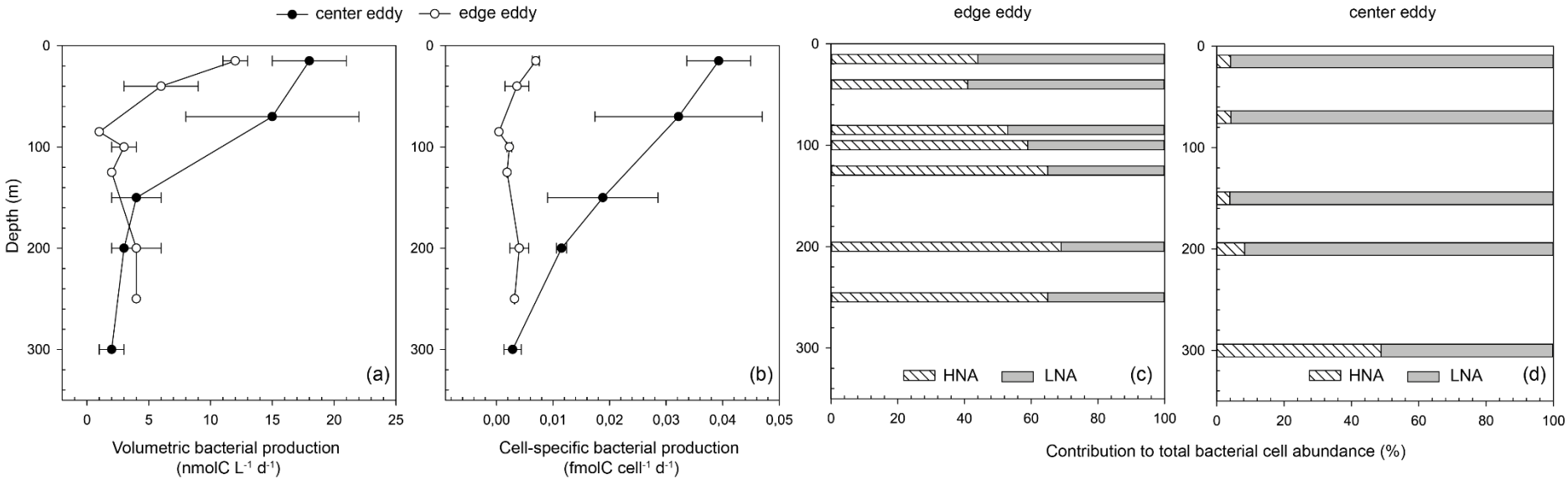

Suppl. Figure 4 Depth profiles of bacterial production and abundance at the center and at the edge of the eddy. Profiles of volumetric **(a)** and cell-specific (relative to cell abundance) bacterial production **(b)** versus depth. Error bars represent 1 standard deviation for replicate measurements. Percent of relative contribution of high DNA content (HNA) and low DNA content (LNA) cells to total bacterial abundance at the edge **(c)** and center **(d)** of the eddy.

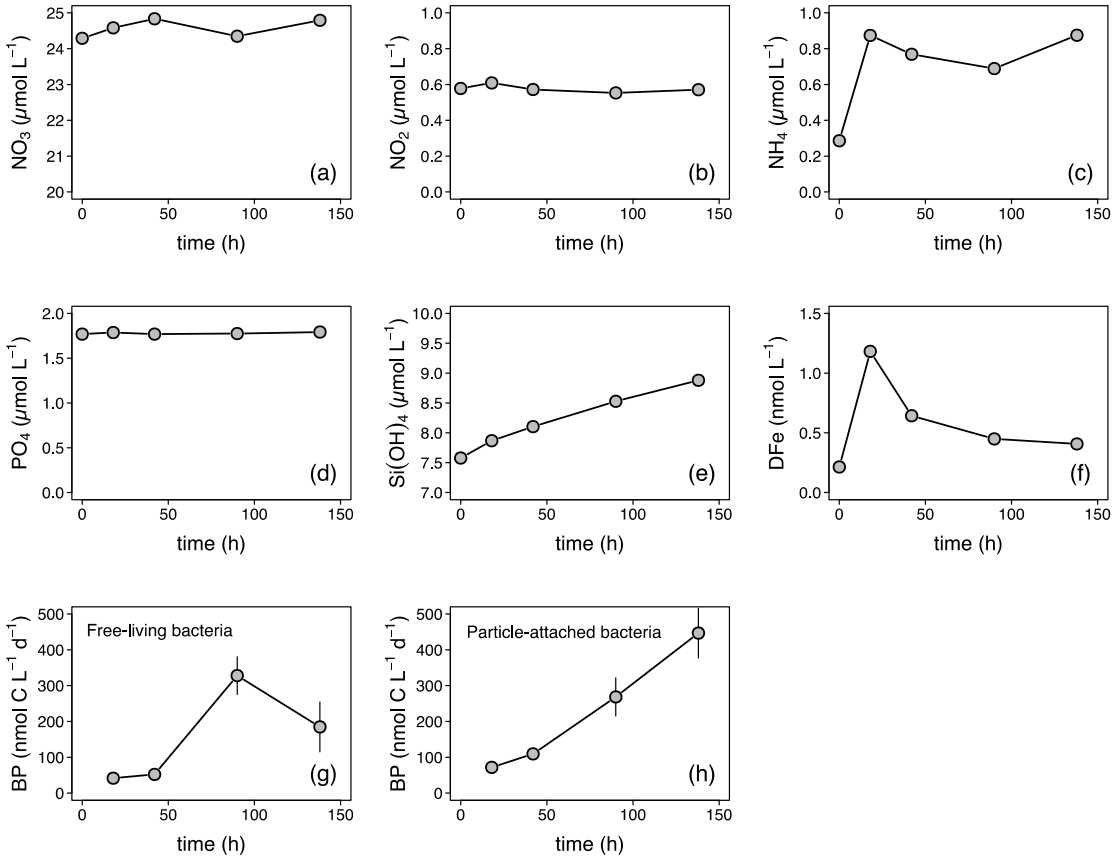

Suppl. Figure 5. Time evolution of dissolved (**a**) nitrate, (**b**) nitrite, (**c**) ammonium, (**d**) phosphate, (**e**) silicate, and (**f**) iron concentrations, and production by (**g**) free-living and (**h**) particle-attached heterotrophic bacteria during the remineralization of subsurface particles (section 2.1). Particle-attached BP was obtained by subtracting the free-living (<1-µm) from the total (unfiltered) BP.

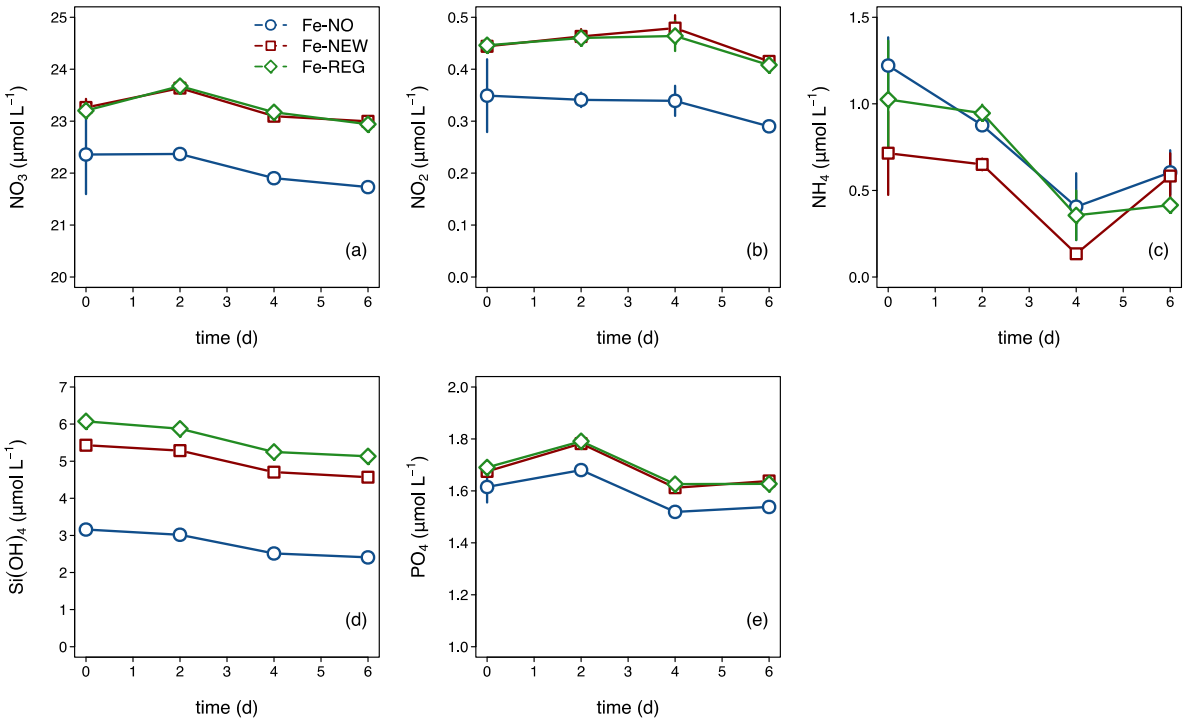

Suppl. Figure 7. Time evolution of dissolved inorganic (**a**) nitrate, (**b**) nitrite, (**c**) ammonium, (**d**) silicate, and (**e**) phosphate concentrations during the incubation. Error bars represent the standard deviation of three incubation bottle replicates.

Suppl. Table 1. Initial biogeochemical conditions for the Fe-NO, Fe-NEW, and Fe-REG treatments.

	Fe-NO	**Fe-NEW**	**Fe-REG**
Ammonium (μM)	1.22 ± 0.16	0.72 ± 0.24	1.03 ± 0.34
Nitrate (μM)	22.36 ± 0.76	23.26 ± 0.17	23.20 ± 0.03
Nitrite (μM)	0.35 ± 0.07	0.44 ± 0.01	0.45 ± 0.01
Phosphate (μM)	1.62 ± 0.06	1.68 ± 0.01	1.69 ± 0.01
Silicate (μM)	3.16 ± 0.08	5.43 ± 0.01	6.07 ± 0.07
Dissolved iron (nM)	0.11 ± 0.01	0.16 ± 0.04	0.26 ± 0.02
Chlorophyll-a (μg L^{-1})	0.154 ± 0.016	0.132 ± 0.015	0.132 ± 0.003
F_v/F_m	0.52 ± 0.05	0.50 ± 0.05	0.44 ± 0.04

Suppl. Table 2. Iron and carbon uptake rates for the different components of the in-eddy phytoplankton community (from companion paper Ellwood et al. 2020).

	0.2-2-μm [a,b]	2-20-μm [a,b]	>20-μm [a,b]
Fe uptake (pmol L^{-1} d^{-1})	17.4 (5.6)	4.6 (3.0)	4.9 (1.2)
C uptake (μmol L^{-1} d^{-1})	0.06 (0.01)	0.05 (0.03)	0.04 (0.01)
Fe:C ratio (μmol mol^{-1})	285.4 (92.5)	99.6 (88.9)	120.6 (43.3)

[a] incubation at 80% incident irradiance; [b] extracellular Fe removed using Ti(III) EDTA-citrate

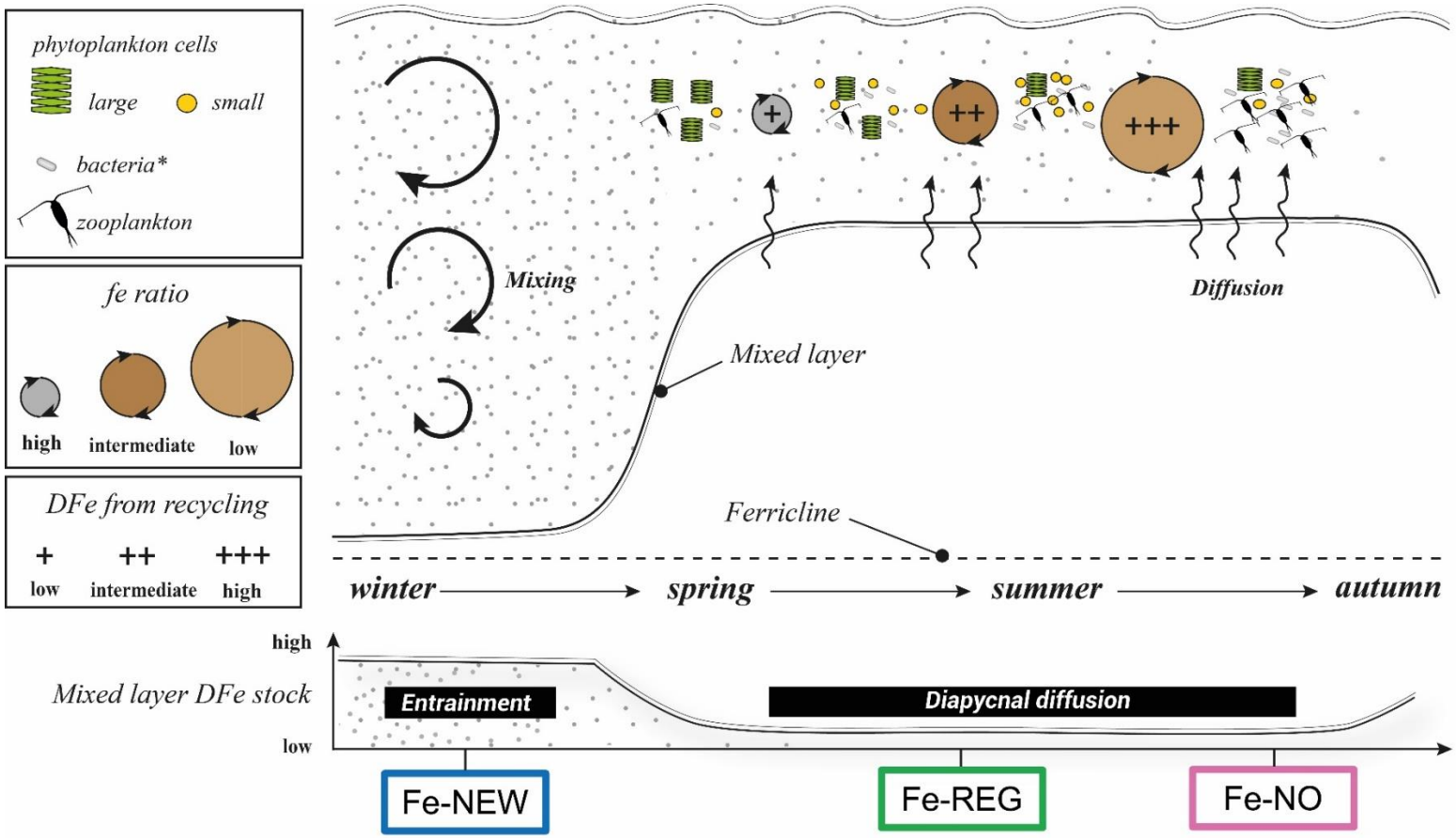

Suppl. Figure 1 A schematic representation of the seasonal variability in Southern Ocean Fe cycling adapted from Tagliabue et al. 2014. Seasonal changes in the physical supply of DFe (black arrows), mixed-layer depth and the mixed-layer DFe inventory are emphasized. The magnitude of recycling and changes in *f*e ratio are presented together (circles and cross) as well as a simplified view of the pelagic community composition. The dominant physical processes over the season is conceptualized at the bottom of the figure with the evolution of DFe inventories in the mixed layer. DFe sources (Fe-NEW, Fe-REG, and Fe-NO) used in this study aim to represent the seasonal transition of modes of DFe supply from mainly new DFe early in the season (entrainment) to regenerated DFe from recycle of sinking materials later during the summer (diapycnal diffusion) and no DFe supply.

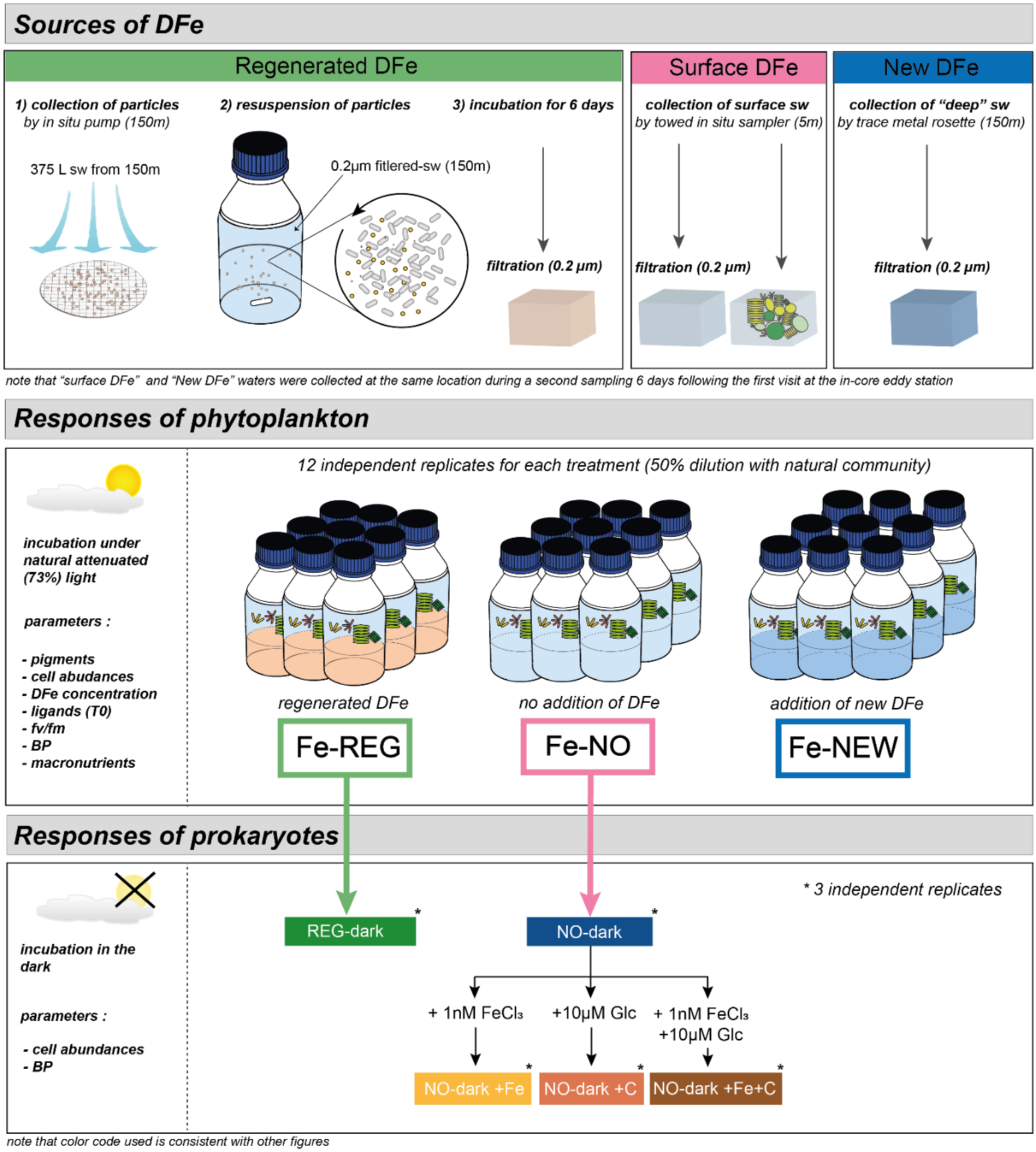

Suppl. Figure 2. A schematic representation of the experimental set-up.

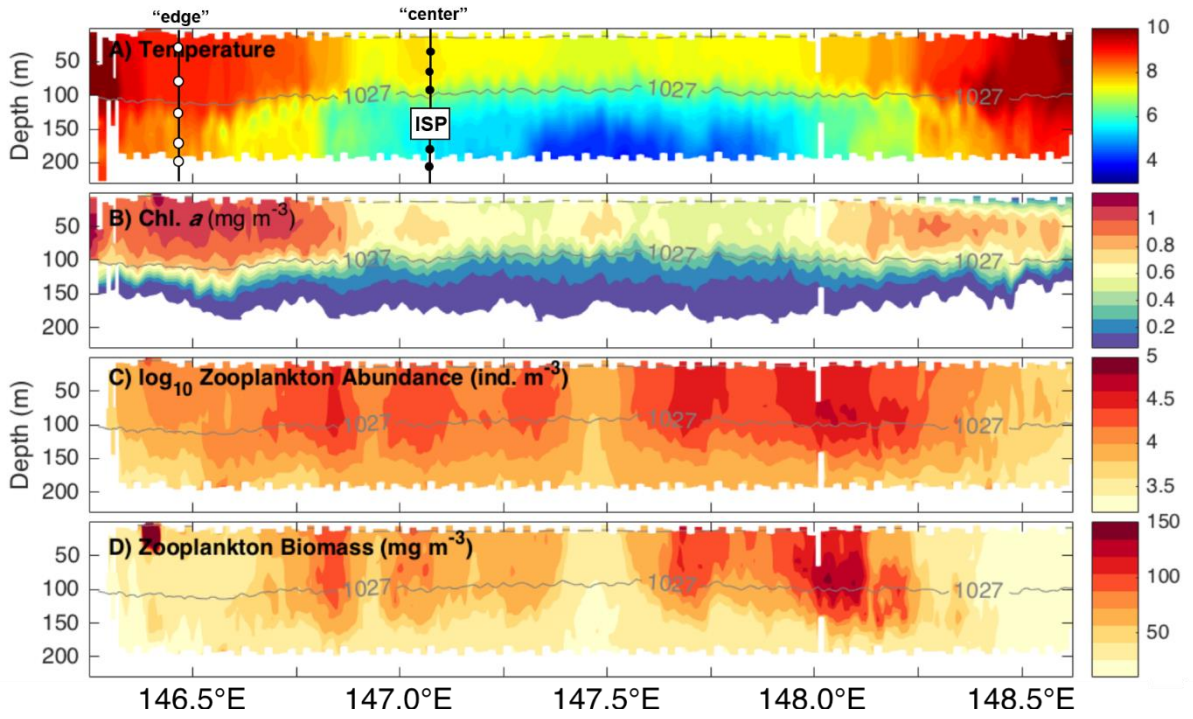

Suppl. Figure 3 (**a**) Temperature, (**b**) Chl a concentration, and zooplankton (**c**) abundance and (**d**) biomass (obtained from a Laser Optical Plankton Recorder) within the cold-core eddy and at the eddy's periphery. Location of the sampling for bacterial production profiles at the periphery ("edge", white dots) and at the within the eddy ("center", black dots) are shown in (a) panel. Sampling for surface (5m) microbial community was done at same location within the eddy ("center") as the collection of subsurface particles by In Situ Pump (ISP) deployed at 150m depth.

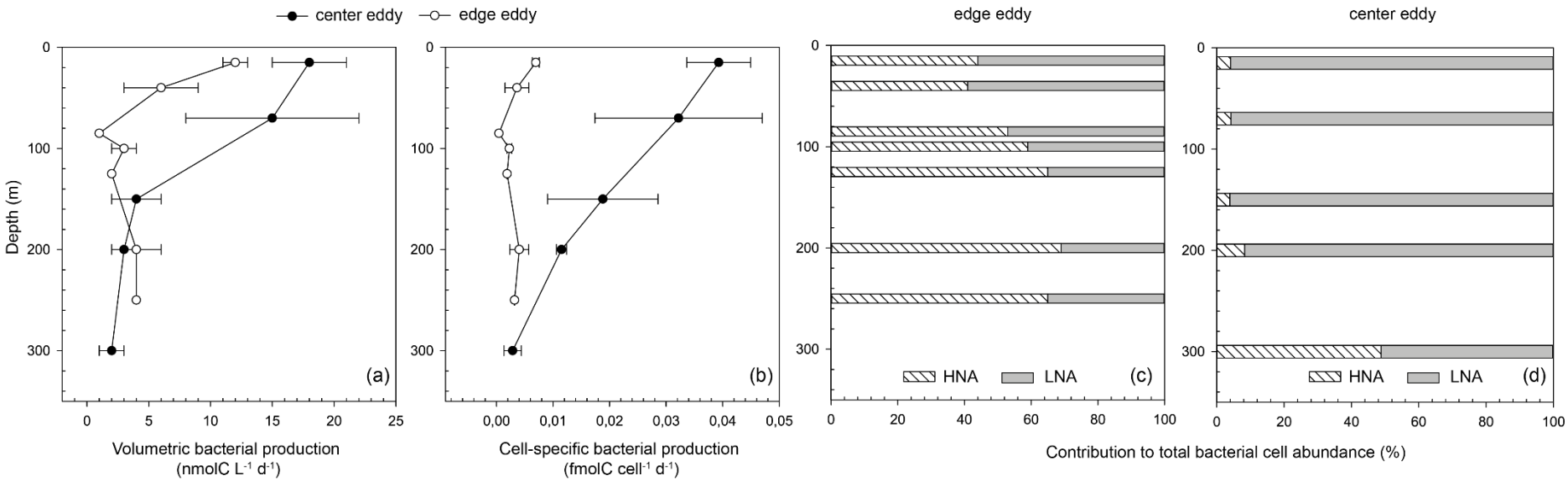

Suppl. Figure 4 Depth profiles of bacterial production and abundance at the center and at the edge of the eddy. Profiles of volumetric **(a)** and cell-specific (relative to cell abundance) bacterial production **(b)** versus depth. Error bars represent 1 standard deviation for replicate measurements. Percent of relative contribution of high DNA content (HNA) and low DNA content (LNA) cells to total bacterial abundance at the edge **(c)** and center **(d)** of the eddy.

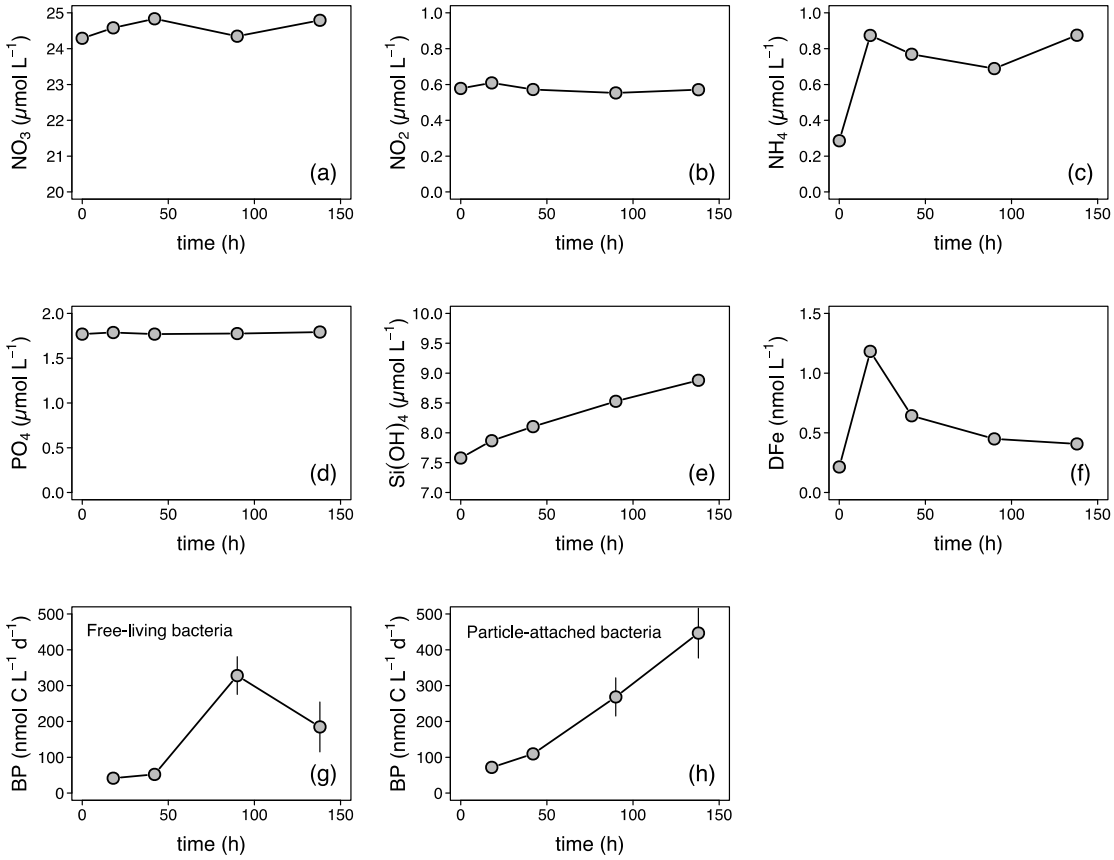

Suppl. Figure 5. Time evolution of dissolved (**a**) nitrate, (**b**) nitrite, (**c**) ammonium, (**d**) phosphate, (**e**) silicate, and (**f**) iron concentrations, and production by (**g**) free-living and (**h**) particle-attached heterotrophic bacteria during the remineralization of subsurface particles (section 2.1). Particle-attached BP was obtained by subtracting the free-living (<1-µm) from the total (unfiltered) BP.

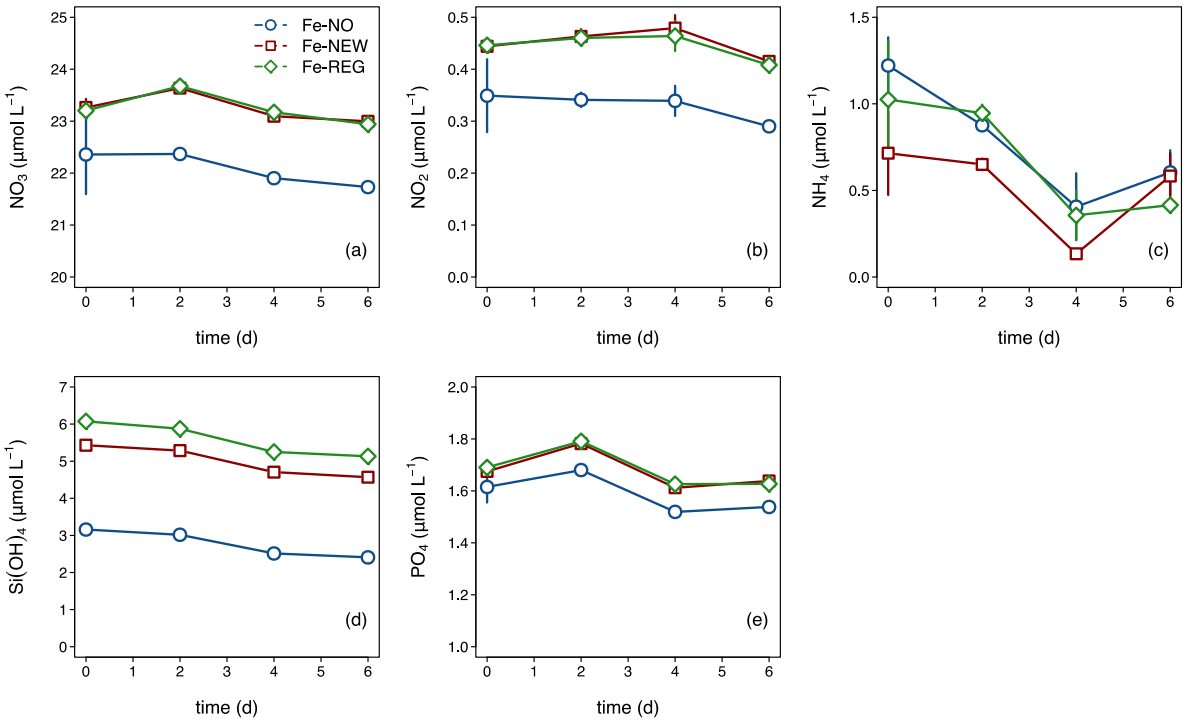

Suppl. Figure 7. Time evolution of dissolved inorganic (**a**) nitrate, (**b**) nitrite, (**c**) ammonium, (**d**) silicate, and (**e**) phosphate concentrations during the incubation. Error bars represent the standard deviation of three incubation bottle replicates.